

<sup>1</sup> **GLO-Roots: an imaging platform enabling multidimensional characterization of soil-grown roots systems**

<sup>3</sup> Rubén Rellán-Álvarez<sup>1, 9</sup>, Guillaume Lobet<sup>2</sup>, Heike Lindner<sup>1, 8</sup>, Pierre-Luc Pradier<sup>1, 8, 10</sup>,  
<sup>4</sup> Jose Sebastian<sup>1, 8</sup>, Muh-Ching Yee<sup>1</sup>, Yu Geng<sup>1, 7</sup>, Charlotte Trontin<sup>1</sup>, Therese LaRue<sup>3</sup>,  
<sup>5</sup> Amanda Schrager-Lavelle<sup>4</sup>, Cara H. Haney<sup>5</sup>, Rita Nieu<sup>6</sup>, Julin Maloof<sup>4</sup>, John P. Vogel<sup>7</sup>,  
<sup>6</sup> José R. Dinneny<sup>1, 12</sup>

<sup>7</sup> <sup>1</sup> Department of Plant Biology, Carnegie Institution for Science, Stanford, CA, USA.

<sup>8</sup> <sup>2</sup> PhytoSystems, University of Liège, Liège, Belgium.

<sup>9</sup> <sup>3</sup> Department of Biology, Stanford University, Stanford, CA, USA.

<sup>10</sup> <sup>4</sup> Department of Plant Biology, UC Davis, Davis, CA, USA.

<sup>11</sup> <sup>5</sup> Harvard Medical School, Massachusetts General Hospital, Department of Genetics, De-  
<sup>12</sup> partment of Molecular Biology Boston, MA, USA

<sup>13</sup> <sup>6</sup> USDA Western Regional Research Center, Albany, CA, USA

<sup>14</sup> <sup>7</sup> DOE Joint Genome Institute, Walnut Creek, CA, USA

<sup>15</sup> <sup>8</sup> These authors contributed equally

<sup>16</sup> <sup>9</sup> Present address: Laboratorio Nacional de Genómica para la Biodiversidad (Langebio),  
<sup>17</sup> Unidad de Genómica Avanzada, Centro de Investigación y de Estudios Avanzados del Insti-  
<sup>18</sup> tuto Politécnico Nacional (CINVESTAV-IPN), Irapuato, Guanajuato, México

<sup>19</sup> <sup>10</sup> Present address: Boyce Thompson Institute for Plant Research/USDA, Ithaca, NY, USA.

<sup>20</sup> <sup>11</sup> Present address: Energy Biosciences Institute, UC, Berkeley, CA, USA

<sup>21</sup> <sup>12</sup> Corresponding author

<sup>22</sup> **Author contributions:**

<sup>23</sup> RR-A: Conception, design and development of the growth and imaging system and Arabidop-  
<sup>24</sup> sis transgenic lines; acquisition, analysis and interpretation of data; drafting and revising

25 the article.

26 GL: Development of the GLO-RIA image analysis plugin, analysis and interpretation of

27 data, drafting and revising the article.

28 HL: Acquisition of data, development of the tomato growth and imaging setup.

29 P-LP: Acquisition of data, analysis and interpretation of data

30 JS: Development of Brachypodium transgenic lines, acquisition and analysis of Brachy-

31 podium, Arabidopsis and tomato data.

32 MCY: Development of Arabidopsis and Brachypodium transgenic lines.

33 YG: Development of Arabidopsis transgenic lines.

34 CT: Acquisition and analysis of the QPCR data

35 TL: Acquisition and analysis of the QPCR data

36 AS-L: Contributed the unpublished dual-color tomato line.

37 CH: Contributed the unpublished *Pseudomonas fluorescens* CH267-lux strain.

38 RN: Contribution to the development of the Brachypodium transgenic line.

39 JM: Contributed the unpublished dual-color tomato line.

40 JPV: Contribution to the development of the Brachypodium transgenic line.

41 JRD: Conception, design and development of the growth and imaging system and Arabidop-

42 sis transgenic lines; acquisition, analysis and interpretation of data; drafting and revising

43 the article.

44 All authors read and approve the final version of the manuscript.

45 **Abstract**

46 Root systems develop different root types that individually sense cues from their local

47 environment and integrate this information with systemic signals. This complex multi-

48 dimensional amalgam of inputs enables continuous adjustment of root growth rates, direc-  
49 tion and metabolic activity that define a dynamic physical network. Current methods for  
50 analyzing root biology balance physiological relevance with imaging capability. To bridge  
51 this divide, we developed an integrated imaging system called Growth and Luminescence  
52 Observatory for Roots (GLO-Roots) that uses luminescence-based reporters to enable stud-  
53 ies of root architecture and gene expression patterns in soil-grown, light-shielded roots. We  
54 have developed image analysis algorithms that allow the spatial integration of soil prop-  
55 erties such as soil moisture with root traits. We propose GLO-Roots as a system that  
56 has great utility in presenting environmental stimuli to roots in ways that evoke natural  
57 adaptive responses and in providing tools for studying the multi-dimensional nature of such  
58 processes.

## 59 **Introduction**

60 Plant roots are three-dimensional assemblies of cells that coordinately monitor and acclimate  
61 to soil environmental change by altering physiological and developmental processes through  
62 cell-type and organ-specific regulatory mechanisms<sup>1,2</sup>. Soil comprises a complex distribution  
63 of particles of different size, composition and physical properties, airspaces, variation in  
64 nutrient availability and microbial diversity<sup>3,4</sup>. These physical, chemical and biological  
65 properties of soil can vary on spatial scales of meters to microns, and on temporal scales  
66 ranging from seasonal change to seconds. Root tips monitor this environment through  
67 locally and systemically acting sensory mechanisms<sup>5,6</sup>.

68 The architecture of the root system determines the volume of soil where resources can be  
69 accessed by the plant (rhizosphere) and is under both environmental and genetic control.  
70 Plasticity in growth parameters allows the plant to adjust its form to suit a particular soil.  
71 Lateral roots, which usually make up the majority of the total root system, often grow at an  
72 angle divergent from the gravity vector. This gravity set-point angle (GSA) is controlled by  
73 auxin biosynthesis and signaling and can be regulated by developmental age and root type<sup>7</sup>.  
74 Recent cloning of the *DRO1* Quantitative Trait Locus (QTL) demonstrates that natural

75 genetic variation is a powerful tool for uncovering such control mechanisms<sup>8</sup>.

76 Specific root ideotypes (idealized phenotypes) have been proposed to be optimal for acquisi-  
77 tion of water and nitrogen, which are distinct from ideotypes for low phosphorus. Based on  
78 computational modeling and field studies, the “steep, deep and cheap” ideotype proposed by  
79 Lynch and colleagues may provide advantages to the plant for capturing water and elements  
80 like nitrogen that are water soluble and therefore tend to move in the soil column with water.  
81 This ideotype consists of highly gravitropic, vertically oriented roots that grow deep in the  
82 soil column and develop large amounts of aerenchyma, which reduces the overall metabolic  
83 cost of the root system<sup>3</sup>. Other nutrients, like phosphorus, which have limited water solu-  
84 bility and are tightly bound to organic matter, usually accumulate in the top layers of soil  
85 and favor root systems that are more highly branched and shallow. The low-phosphorus  
86 ideotype effectively increases root exploration at the top layers of soil<sup>3</sup>. Modeling of root  
87 system variables shows that optimum architecture for nitrogen and phosphorus uptake are  
88 not the same<sup>9</sup> and suggests tradeoffs that may affect the evolution of root architecture as a  
89 population adapts to a particular environmental niche.

90 Clearly, understanding the architecture of root systems and how environmental conditions  
91 alter root developmental programs is important for understanding adaptive mechanisms of  
92 plants and for identifying the molecular-genetic basis for different response programs. In  
93 addition, root systems have complexity beyond their architecture that needs to be incorpo-  
94 rated into our understanding of plant-environment interactions. Primary and lateral roots  
95 exhibit different stress response programs in *Arabidopsis*<sup>2</sup> and may play specialized roles  
96 in water and nutrient uptake. Thus, it is important to develop methods that allow for a  
97 multidimensional characterization of the root system that includes growth, signaling, and  
98 interactions with other organisms. Furthermore, physiological parameters that affect whole  
99 plant responses to the environment, such as transpiration, are likely integrated into such  
100 processes, thus requiring a more holistic approach to studies of root function.

101 Based on these considerations we have developed a new root imaging platform, Growth  
102 and Luminescence Observatory for Roots (GLO-Roots), which allows root architecture and

103 gene expression to be studied in soil-grown plants. GLO-Roots is an integrated system  
104 composed of custom growth vessels, luminescent reporters and imaging systems. We use  
105 rhizotrons that have soil volumes equivalent to small pots and support growth of Arabidopsis  
106 from germination to senescence. To visualize roots, we designed plant-codon optimized  
107 luciferase reporters that emit light of different wavelengths. To visualize reporter expression,  
108 plants are watered with a dilute luciferin solution and imaged afterwards. We have built  
109 a custom luminescence imaging system that automatically captures images of rhizotrons  
110 held vertically. The signal from each reporter is distinguished using band-pass filters held  
111 in a motorized filter wheel, which enables automated acquisition of images from plants  
112 expressing both structural and environmentally and developmentally responsive reporters.  
113 We have also developed GLO-RIA (GLO-Roots Image Analysis), an ImageJ<sup>10</sup> plugin that  
114 allows for automated determination of root system area, convex hull, depth, width and  
115 directionality, which quantifies the angle of root segments with respect to gravity. GLO-  
116 RIA is also able to relate root system parameters to local root-associated variables such as  
117 reporter expression intensity and soil-moisture content.

118 Overall GLO-Roots has great utility in presenting environmental stimuli to roots in phys-  
119 iologically relevant ways and provides tools for characterizing responses to such stimuli at  
120 the molecular level in whole adult root systems over broad time scales.

### 121 **Box 1.**

122 All resources for GLO-Roots, including the original raw data used in the manuscript, sample  
123 images, GLO-RIA user manual, the latest software updates and the source code, can be  
124 found at: <https://dinnenylab.wordpress.com/glo-roots/>

### 125 **Results**

126 We have developed an integrated platform for growing, imaging and analyzing root growth  
127 that provides advances in physiological relevance and retains the ability to visualize aspects

<sup>128</sup> of root biology beyond structure.

<sup>129</sup> **The GLO-Roots platform**

<sup>130</sup> GLO-Roots is comprised of four parts: i) growth vessels called rhizotrons that allow plant  
<sup>131</sup> growth in soil and root imaging; ii) luminescent reporters that allow various aspects of root  
<sup>132</sup> biology to be tracked in living plants; iii) GLO1 luminescence-imaging system designed to  
<sup>133</sup> automatically image rhizotrons; iv) GLO-RIA, an image analysis suite designed to quantify  
<sup>134</sup> root systems imaged using GLO-Roots.

<sup>135</sup> **Plant growth system** GLO-Roots utilizes custom designed growth vessels classically  
<sup>136</sup> known as rhizotrons, which hold a thin volume of soil between two sheets of polycarbon-  
<sup>137</sup> ate plastic. Acrylic spacers provide a 2-mm space in which standard peat-based potting  
<sup>138</sup> mix is added. Black vinyl sheets protect roots from light and rubber U-channels clamp  
<sup>139</sup> the rhizotron materials together. Plastic racks hold the rhizotrons vertically and further  
<sup>140</sup> protect the roots from light. Rhizotrons and rack are placed in a black tub and water are  
<sup>141</sup> added, to a depth of about 2 cm, at the bottom to maintain moisture in the rhizotrons  
<sup>142</sup> during plant growth. The volume of soil in the rhizotrons ( $100 \text{ cm}^3$ ) is similar to small pots  
<sup>143</sup> commonly used for *Arabidopsis* and supports growth throughout the entire life cycle (Fig  
<sup>144</sup> 1A-C and Supplement 1). To determine how the biology of plants grown in rhizotrons com-  
<sup>145</sup> pares to other standard growth systems, we utilized high-throughput qRT-PCR to study  
<sup>146</sup> how these conditions affect expression of 77 marker genes in root and shoot samples. These  
<sup>147</sup> genes were curated from the literature and belong to a wide array of biological pathways  
<sup>148</sup> including nutrient acquisition, hormone and light response and abiotic stress. Whole roots  
<sup>149</sup> and shoot samples were collected at the end of the light and dark periods (Long-day condi-  
<sup>150</sup> tions: 16 hour light, 8 hours dark) from plants grown in rhizotrons, pots, and petri dishes  
<sup>151</sup> with two different media compositions (1X Murashige and Skoog basal salts (MS), 1% su-  
<sup>152</sup> crose or 0.25X MS, no sucrose). Principal component analysis of the gene expression values  
<sup>153</sup> showed a separation of soil and gel-grown root systems in the the first principal compo-  
<sup>154</sup> nents (Figure 1-figure supplement 1A). In roots grown on gel-based media, we observed

enhanced expression of genes associated with light-regulated pathways (flavonoid biosynthesis: *FLAVINOL SYNTHASE1*, *FLS1*, *CHALCONE SYNTHASE*, *CHS* and photosynthesis: *RUBISCO SUBUNITS1A*, *RBCS1A*, *CYCLOPHILIN 38*, *CYP38*), which is expected due to the exposure of gel-grown roots to light. In addition, genes associated with phosphorus nutrition (*LOW PHOSPHATE RESPONSE1*, *LPR1*, *PHOSPHATE STARVATION RESPONSE1*, *PHR1*) were (Figure 1-figure table supplement 1) less expressed in soil-grown roots, suggesting differences in nutrient availability between the different growth systems. Interestingly, shoot samples were not clearly distinguished by growth media and, instead, time of day had a greater effect (Figure 1-Supplement 2). These data suggest root systems may be particularly sensitive to media conditions and indicate that rhizotron-grown root systems more closely approximate the biology of pot-grown plants than standard gel-based media. Shoot weight and primary root length were significantly reduced for gel-grown plants compared to rhizotron- or pot-grown plants suggesting significant differences in the biology of plants grown under these conditions (Figure 1-figure supplement 1B-C). While the 2 mm depth of the soil sheet is 10 to 20 times the average diameter of an Arabidopsis root (between 100-200 microns<sup>11</sup>), we evaluated whether rhizotron-grown plants exhibited any obvious stress as a consequence of physical constriction. We compared traits of plants growing in vessels that hold similar volumes of soil but in different volumetric shapes. The number of lateral roots was significantly lower in pot and cylinder-grown plants compared to rhizotron-grown plants (Figure 1-figure supplement 1D) whereas primary root length of rhizotron and cylinder-grown plants was significantly greater than pot-grown plants (Figure 1-figure supplement 1E). No significant differences in shoot area were observed between the three systems (Figure 1-figure supplement 1-data). Thus, these data do not support the hypothesis that rhizotron-grown plants experience physical constriction greater than other vessels holding the same volume of soil.

**Generation of transgenic plants expressing different luciferases** Arabidopsis roots cannot easily be distinguished from soil using brightfield imaging due to their thinness and translucency (Figure 1-figure supplement 3); thus, reporter genes are needed to enhance the

183 contrast between the root and their environment. Luciferase is an ideal reporter to visualize  
184 roots: 1) unlike fluorescent reporters, luciferase does not require high-intensity excitation  
185 light, which could influence root growth, 2) peat-based soil (a type of histosol) exhibits no  
186 autoluminescence but does autofluoresce at certain excitation wavelengths similar to GFP  
187 (Figure 1-figure supplement 3), 3) while GFP is very stable, and thus not as suitable for  
188 imaging dynamic transcriptional events, the luciferase enzyme is inactivated after catabolism  
189 of luciferin, making it ideal for studying processes such as environmental responses. A  
190 considerable number of luciferases have been developed that emit light spanning different  
191 regions of the visible spectrum, but their utilization has been limited to studies in animals  
192 (Table 1).

193 To determine the efficacy of using luciferase to visualize roots in soil, we codon optimized  
194 sequences of *PpyRE8*, *CBGRed*, *LUC2*, and *CBG99* for Arabidopsis expression. In addition,  
195 nanoLUC and venus-LUC<sup>12</sup> were utilized. Constitutive luciferase expression was driven  
196 in plants using the *UBIQUITIN 10* (*UBQ10*) or *ACTIN2* (*ACT2*) promoters using vectors  
197 assembled through a Golden-Gate cloning system<sup>13</sup>. Plants homozygous for a single locus  
198 T-DNA insertion were evaluated for in vivo emission spectra and luminescence intensity  
199 (Fig 1D). All the evaluated luciferases use D-luciferin as a substrate facilitating the simulta-  
200 neous imaging of different luciferases except nanoLUC, which uses a proprietary substrate  
201 furimazine<sup>14</sup>. In general, luciferases with red-shifted emission spectra were less intense than  
202 the green-shifted luciferases (Fig 1D). LUC2o showed an emission maximum at 580 nm and  
203 a minor peak at 620 nm while CBG99o lacks the minor peak.

204 Continuous addition of luciferin did not have any significant effect on shoot weight or primary  
205 root length (Figure 1-figure supplement 4). After luciferin addition, luminescence signal  
206 could be reliably detected in root systems for up to 10 days, depending on the developmental  
207 state of the plant.

208 **GLO1: a semi-automated luminescence imaging system for rhizotrons** Lumines-  
209 cence imaging systems commercially available for biomedical research are usually optimized

for imaging horizontally held specimens or samples in microtiter plates. Placing rhizotrons in this position would induce a gravitropic response in plants. Working with Bioimaging Solutions (San Diego, CA) we designed and built a luminescence imaging system optimized for rhizotron-grown plants. GLO1 (Growth and Luminescence Observatory 1) uses two back-thinned CCD cameras (Princeton Instruments, USA) to capture partially-overlapping images of rhizotrons while a motorized stage automatically rotates the rhizotron to capture images of both sides (Fig 1E). A composite image is generated from the images captured of each side; Fig 1F shows that approximately half of the root system is revealed on each side with few roots being visible on both sides. Apparently, the soil sheet is thick enough to block portions of the root system but thin enough to ensure its continuous structure can be compiled from opposite face views. We tested the ability of GLO1-generated images to reveal complete root systems by manually quantifying the number of lateral roots in excavated root systems of 8 different plants and testing these results against estimates of lateral root number from images of the same plants visually inspected by 4 different persons. These comparisons revealed good correlation ( $(R^2 = 0.974)$ ) between actual lateral root counts and image-based estimation, indicating GLO1-generated root images provide an accurate representation of the in soil root system.

**GLO-RIA: GLO-Roots Image Analysis** We developed a set of image analysis algorithms that were well suited for the complex root systems that GLO-Roots is able to capture. GLO-RIA (Growth and Luminescence Observatory Root Image Analysis) is an ImageJ plugin divided in two modules. The first module (RootSystem) performs four different types of analysis: i) a local analysis that detects all root particles in the image and computes their position, length and direction; ii) the global analysis performs a root system level analysis and computes the total visible surface, convex hull, width and depth; iii) the shape analysis uses Elliptic Fourier Descriptors or pseudo-landmarks similarly to RootScape<sup>15</sup> to perform a shape analysis on the root system iv) the directionality analysis computes the mean direction of root particles in a root system (either on the full image or by a user-defined region of interest in the image). These four analysis methods are fully automated by default, but

238 can be manually adjusted if needed. The second module of GLO-RIA (RootReporter) was  
239 specifically designed for the analysis of multi-layered images such as combinations of gene  
240 reporter, root structure and soil moisture. Shortly, the plugin works as follows: i) detection  
241 of the gene reporters and the structure reporters in their respective images; ii) if needed, a  
242 manual correction can be performed to correct the automated detection; iii) gene reporters  
243 are linked with the soil water content and the structure reporters, based on their proximity;  
244 iv) gene reporter intensity (either absolute or normalized using the structural reporter) is  
245 computed; v) all data are exported and saved to a RSML datafile<sup>16</sup>. Gene and structure  
246 reporters can be followed across different time and space points. Using an object oriented  
247 approach, great care has been taken to facilitate the user interactions on the different images  
248 to streamline the analysis process. Table 2 shows a list of root system features extracted  
249 using GLO-RIA. GLO-RIA does not currently have the ability to reconstruct the root archi-  
250 tecture in itself (topological links between roots). This is a challenge for analyzing images  
251 captured by GLO-Roots since soil particles cause disruption of root segments.

252 **Continuous imaging of root growth**

253 The size of our rhizotrons enables undisturbed root system development (before roots reach  
254 the sides or the bottom of the rhizotron) for about 21-23 days for the Col-0 accession  
255 growing under long day conditions (Figure 2); however root traits such as directionality  
256 can be observed through later stages of plant development. See 35 DAS root system and  
257 directionality in Figure 2A-B. An example of a time series spanning 11 to 21 days after  
258 sowing (DAS) of Col-0 roots expressing *ProUBQ10:LUC2o* is shown in Fig 2A and [Video 1](#)  
259 with a color-coded time projection shown in Fig 2C. Directionality analysis (Fig 2B) shows  
260 a progressive change in root system angles from 0 ° (vertical) to 45 ° as lateral roots take  
261 over as the predominant root type. Figure 2D shows the evolution over time of several root  
262 traits that can be automatically captured by GLO-RIA (depth, width, area) and others that  
263 were manually quantified (primary root growth rate or number of lateral roots per primary  
264 root).

265    #### Root system architecture of different *Arabidopsis* accessions.

266    As a proof of concept to estimate the utility of our root imaging system to phenotype  
267    adult root system traits, we transformed a small set of accessions (Bay-0, Col-0 and Sha)  
268    with the *ProUBQ10:LUC2o* reporter and quantified RSA at 22 DAS (Fig 3A-C). GLO-RIA  
269    analysis of these root systems identified several root traits that distinguish Col-0, Bay-0  
270    and Sha. Directionality analysis revealed an abundance of steep-angle regions in the root  
271    system of Bay while Sha showed an abundance of shallow-angled regions and Col-0 was  
272    intermediate (Fig 3D). Bay-0 shows the deepest and narrowest root system leading to the  
273    highest depth/width ratio while Sha has the widest root system (Fig 3E). Other root traits  
274    such as root system area and the vertical center of mass also showed significant differences  
275    (Figure 3-figure supplement 1B). Broad sense heritability values for depth (96.3), area (92.0),  
276    depth/width (97.8), width (95.7) and vertical center of mass (95.0) were all higher than 90%.  
277    To capture the richness of root architecture shape, we used GLO-RIA to extract pseudo-  
278    landmarks describing the shape of the root system (see Materials and Methods for more  
279    details) and performed PCA analysis. The first principal component captures differences  
280    in the distribution of widths along the vertical axis and separates Col-0 and Sha from Bay-  
281    0 root systems. (Fig 3F). Bay-0 shows an homogenous distribution of widths along the  
282    vertical axis while Sha and Col-0 are much wider at the top than bottom. PC2 seems to be  
283    capturing a relationship between width at the top and total depth and separates Sha root  
284    systems which are wide at the top and deep from Col-0 root systems which are wide but  
285    not as deep as Sha. Shape information extracted from pseudo-landmarks can distinguish  
286    the three different accession using PCA analysis (Fig 3G)

287    **Spectrally distinct luciferases enable gene expression patterns, characterization  
288    of root system interactions and microbial colonization.**

289    We tested whether spectrally distinct luciferase reporters would enable additional informa-  
290    tion besides root architecture to be captured from root systems. Luciferase reporters have  
291    been commonly used to study gene expression and these resources can potentially be utilized

292 to study such regulatory events in soil-grown roots. We transformed *ProACT2:PpyRE8o*  
293 into two well studied LUC reporter lines: the auxin response reporter line *ProDR5:LUC+*<sup>17</sup>  
294 (Figure A-B) and the Reactive Oxygen Species (ROS) response reporter *ProZAT12:LUC*<sup>18</sup>  
295 (Figure 4C-D). We implemented in GLO-RIA an algorithm that semi-automatically iden-  
296 tifies gene reporter signal and associates this object to the corresponding root structure  
297 segment. A graphical representation of the results obtained with Root Reporter can be  
298 observed in Figure 4-figure supplement 1. Reporter intensity values along the first 5 mm  
299 of root tips can also be observed in Figure 4-figure supplement 2. We then took advantage  
300 of our ability to constitutively express two spectrally different luciferases and imaged the  
301 overlapping root systems (one expressing *ProUBQ10:LUC2o* and the other *ProACT2:PPy*  
302 *RE8o*). While two root systems were distinguishable using this system (Figure 4-figure sup-  
303 plement 3); measurements of root system area did not reveal a significant effect on root  
304 growth when two plants were grown in the same rhizotron, compared to one; however, fur-  
305 ther studies are warranted (Figure 4-figure supplement 3).

306 The GLO-Roots system uses non-sterile growth conditions, which allows complex biotic  
307 interactions that may affect responses to the environment. Bacteria themselves can be en-  
308 gineered to express luminescent reporters through integration of the LUX operon, which  
309 results in luminescence in the blue region of the spectrum and is thus compatible with  
310 the plant-expressed luciferase isoforms we have tested. *Pseudomonas fluorescens* CH267<sup>19</sup>,  
311 a natural *Arabidopsis* root commensal, was transformed with the bacterial LUX operon  
312 and used to inoculate plants. Thirteen days after inoculation, we were able to observe  
313 bacterial luminescence colocalizing with plant roots. *P. fluorescens* did not show an ob-  
314 vious pattern of colonization at the root system scale level. As a proof-of-principle test  
315 of the multi-dimensional capabilities of the GLO-Roots system we visualized both *LUC2o*  
316 and *PPyRE8o* reporters in plants and the LUX reporter in bacteria in the same rhizotron  
317 (Figure 4-figure supplement 4).

318 **Adaptive changes in root system architecture under water deprivation, phos-  
319 phorus deficiency and light** To test the utility of the GLO-Roots system to understand

320 response of root systems to environmental stimuli we tested the effects of light and condi-  
321 tions that mimic drought and nutritional deficiency. To examine the effects of light exposure  
322 on the root architecture, the black shields, which normally protect the soil and roots from  
323 light, were removed from the top half of the rhizotrons 10 DAS. Using directionality analysis  
324 we detected a significant increase in the steepness of roots only in the light exposed region of  
325 the rhizotron, while the lower shielded region showed no difference. (Fig 6-figure supplement  
326 3A-B and Fig 6-figure supplement 4). Light can penetrate the top layers of soil<sup>20</sup> and it  
327 has been proposed to have a role in directing root growth specially in dry soils<sup>21</sup> through  
328 the blue light receptor *phot1*. Root directionality was not significantly different between  
329 light and dark-treated roots of the *phot1/2* double mutant suggesting that blue light per-  
330ception is necessary for this response<sup>21,22</sup> (Fig 6-figure supplement 3B-lower panel). These  
331 data highlight the strong effects of light on root system architecture<sup>23</sup>, which GLO-Roots  
332 rhizotrons are able to mitigate.

333 Plants grown in low-P soil showed a significant increase in the width-depth ratio of the root  
334 system compared to plants grown in P-replete soil, as determined using the automated root  
335 system area finder in GLO-RIA (Fig 6-figure supplement 2A-B). Plants under P deficiency  
336 showed an increase in the ratio between root-shoot area (Fig 6-figure supplement 2C) and  
337 higher investment of resources in the development of the root system at the expense of shoot  
338 growth (Fig 6-figure supplement 2D). Root systems of control and P-deficient plants showed  
339 no significant differences in directionality at 22 DAS but at 27 DAS, roots were more hori-  
340 zontally oriented in P-deficient plants (Fig 6-figure supplement 2E). The observed changes in  
341 root architecture are consistent with root system ideotypes that improve phosphorus uptake  
342 efficiency.

343 GLO-Roots is especially well suited for studying water-deficit (WD) responses. First, shoots  
344 are exposed to the atmosphere and vapor pressure deficit (VPD) is maintained at levels that  
345 allow for transpiration of water from the shoot. Second, soil in rhizotrons is exposed to air  
346 at the top and dries basipetally (from the top-down); drying soil increases the volume  
347 occupied by air and reduces contact of root with liquid water, all of which are similar to

348 changes in soil expected in the field during WD. Finally, as peat-based soil dries, its optical  
349 properties change, allowing moisture content to be approximated from bright-field images.  
350 We took advantage of the change in gray-scale pixel intensity to construct a calibration  
351 curve (Figure 5-figure supplement 1) that quantitatively relates gray-scale pixel intensity to  
352 moisture content (Fig 5A); water content can be color coded in images with appropriate  
353 look up tables (Fig 5B). Soil color was not affected by the presence or absence of roots  
354 (Figure 5-figure supplement 2). Using this approach, water content in a rhizotron can be  
355 mapped and visualized in 2D (Fig 5C-D). In the example shown, we can observe that a 22  
356 DAS Bay-0 plant depleted soil-moisture content locally around the the root system (Figure  
357 5E).

358 We performed several trials to simulate WD in our growth system. Plants were germinated,  
359 grown under control conditions then transferred to 29°C and standing water removed from  
360 the container holding the rhizotrons starting at 9 DAS or 13 DAS. Elevated temperature  
361 combined with water deficit is a common stress that modern crops varieties are poorly  
362 adapted to, thus highlighting the importance of examining this combined treatment<sup>24,25</sup>.  
363 Plants were maintained in this WD regime until 22 DAS when luciferin solution was added  
364 and the plants imaged. At 13 DAS, lateral roots near the soil surface are already emerged  
365 (Video 1, Figure 2A) and 9 days of subsequent WD treatment caused lateral roots to show an  
366 increase in gravitropism leading to the development of a root system that were deeper and  
367 more vertically oriented (Fig 6A). Roots of Bay-0 plants showed similar responses, though  
368 the extent of change was less pronounced since Bay-0 roots are normally more vertically  
369 oriented (Fig 6B). Plants transferred at 9 DAS and grown for 13 days under WD showed  
370 less lateral root development in the top layer of soil (Fig 6E). At this time point, lateral roots  
371 start to emerge (Video 1) and early drought may lead to growth quiescence or senescence.  
372 Careful examination of roots in these regions showed evidence of small lateral root primordia  
373 populating the primary root (Figure 6F). After 24 h of re-watering (Figure 6G) these lateral  
374 root primordia reinitiated growth (Figure 6H).

375 Time-lapse imaging of the water deficit response showed that changes in root growth direc-

376 tion occurred ahead of the dry soil front [Video 2](#). Using GLO-RIA we were able correlate  
377 local water moisture contents with the orientation of root segments. With this approach we  
378 observed that root segments in dryer areas of rhizotron grew at steeper root angles (Figure  
379 7) than roots in WW regions, though lateral root angle in wetter regions was also affected.  
380 These data suggest that both local and systemic signaling is likely involved in redirecting  
381 lateral roots deeper during the simulated drought treatments tested here.

382 We also grew plants under WD at control temperatures or under WW conditions at elevated  
383 temperature to test the effects of these individual stresses on root architecture. We observed  
384 that both conditions were sufficient to induce a change in root directionality indicating that  
385 the plant uses similar mechanisms to avoid heat and water-deficit associated stresses (Figure  
386 6-figure supplement 1). We next asked which regulatory pathways controlled the observed  
387 changes in lateral root directionality during simulated drought. Hydrotropism is a known  
388 environmental response that directs root growth towards wet regions of soil. MIZ1 is an  
389 essential regulator of hydrotropism; however *miz1* mutants had no significant effect on water  
390 deficit-induced changes in root directionality, compared to wild type (Fig 6C), indicating  
391 that this response was distinct from hydrotropism. Auxin is an important mediator of  
392 gravitropism and auxin treatment causes lateral roots to grow more vertically<sup>7</sup>. Consistent  
393 with this role for auxin, mutant plants with loss of function in the auxin receptor TIR1, did  
394 not show changes in the root system directionality between WW and WD conditions (Fig  
395 6D).

### 396 **GLO-Roots for Brachypodium and Tomato.**

397 To examine the general applicability of the GLO-Roots system for other species, we intro-  
398 duced LUC2o-expressing reporters into the model grass *Brachypodium distachyon* and the  
399 crop plant *Lycopersicon esculentum* (tomato). Brachypodium is well suited to the GLO-Root  
400 system because, like Arabidopsis, its small size allows mature root systems to be studied in  
401 relatively small soil volumes<sup>26,27</sup>. *LUC2o* driven by the *ZmUb1* promoter was introduced into  
402 Brachypodium using the pANIC vector<sup>28</sup>. Brachypodium roots showed a distinct architec-

ture from Arabidopsis marked by prolific development of secondary and tertiary lateral roots (Fig 8A). This is consistent with other studies that show that Brachypodium has a typical grass root system<sup>27</sup>. Comparison of root system development in rhizotrons with gel-based media showed that root growth is higher in soil than in plates (Figure 8-figure supplement 1). Previous work has suggested that auxin levels in Brachypodium roots is sub-optimal for growth<sup>29</sup>. Pacheco-Villalobos and colleagues suggest that, in Brachypodium, and contrary to what happens in Arabidopsis, ethylene represses *YUCCA* reducing the synthesis of auxin. The reduced growth that we observe in plates and the high levels of ethylene that build up in sealed plates<sup>30</sup> would support this mechanism.

Tomato plants were transformed with *Pro35S:PPyRE8o* and *ProeDR5rev:LUC2* reporters. The plants showed more rapid growth than Arabidopsis or Brachypodium and required fertilizer to prevent obvious signs of stress (reduced growth, anthocyanin accumulation). Root systems were imaged from 17 DAS plants. Roots showed presumptive lateral root primordia marked by DR5-expression (Fig 8C-D). These results show that the GLO-Roots method can be applied to study root systems of plants and will likely be useful for studying root systems of other small to medium sized model plants and for early stages of larger crop plants.

## Discussion

### GLO-Roots enables a multi-dimensional understanding of root biology

Recent studies of root systems has emphasized structural attributes as important contributors of root system function. Indeed, studies examining the role of genetic variants in tolerating abiotic stress have demonstrated the importance of such characteristics<sup>8</sup>. Roots, however, are highly diverse in the biology they perform and a multi-dimensional understanding of root systems, which incorporates differences in signaling, metabolism and microbial association as well as structure, may provide a clearer understanding of the degree to which sub-functionalization of the root system plays a role in important processes such as acclima-

429 tion and efficient resource acquisition.

430 We have developed tools in GLO-Roots that allow for tracking multiple aspects of soil  
431 physicochemical properties and root biology simultaneously. Using GLO-Roots, we are able  
432 to map in 2D coordinates soil physical properties such soil moisture together with root ar-  
433 chitecture traits such as directionality, growth rates and gene expression levels. All this  
434 information is aggregated in layers for each x, y coordinate. Using GLO-RIA we integrate  
435 this multilayer information, leveraging our ability to simultaneously and seamlessly inves-  
436 tigate root responses to environmental stimuli such as soil moisture content. Luciferase  
437 isoforms that emit light at different wavelengths allow for constitutive and regulated pro-  
438 moters to be studied together. Introduction of luciferase reporters into microbes provides  
439 an additional layer of information that provides a readout on the association between or-  
440 ganisms and how this might be affected by environmental conditions. The flexibility of the  
441 GLO-Roots system may enable additional dimensionality to our understanding of root biol-  
442 ogy. Other physical properties such as CO<sub>2</sub> or pH mapping in rhizotrons have already been  
443 enabled by using planar optodes<sup>31</sup>. It may be possible to engineer LUX-based reporters  
444 in microbes that are responsive to extracellular metabolites, creating microbial biosensors,  
445 and integration of such tools may enable root-exudation and nutrition to be analyzed in  
446 soil. Split-Luciferase reporters have been engineered that allow bi-molecular interactions to  
447 be studied. Finally, molecular sensors analogous to FRET sensors, termed BRET-sensors<sup>32</sup>,  
448 may allow metabolite tracking dynamically through the root system. With additional inno-  
449 vation in the development of luciferase reporters, the GLO-Roots systems will likely expand  
450 the repertoire of biological processes that can be studied over an expanded range of devel-  
451 opmental time points and environmental conditions.

452 **Enhanced root growth and gravitropism may constitute an avoidance mechanism  
453 used during water deficit stress**

454 It has been proposed that plants with steep root systems will be better able to tap into deep  
455 water resources and thus perform better under water deprivation. For example in rice, the

456 IR64 paddy cultivar shows shallow root systems in upland fields whereas Kinandang Patong,  
457 an upland cultivar, is deeper rooting<sup>8</sup>. Plants maintain a number of regulatory pathways that  
458 mediate changes in physiology during WD. Enhanced growth of root systems has been well  
459 characterized in field-grown plants; however this has not been recapitulated in studies of gel-  
460 grown Arabidopsis plants. Thus, it has been unclear whether Arabidopsis simply responds  
461 to WD differently. Our results here show that Arabidopsis does indeed maintain a classical  
462 WD response that expands the root system and directs growth downward. Interestingly,  
463 under our stress regime, we did not observe a significant decrease in the relative water  
464 content of shoot tissues (Figure 6-figure supplement 5), suggesting that the changes in root  
465 architecture were sufficient to provide access to deep water and prevent dehydration. Such  
466 changes in root growth are likely regulated through systemic and local signaling that involve  
467 auxin signaling but acts independently of known pathways that control moisture-directed  
468 root growth.

469 **Perspectives and Conclusions**

470 Understanding plant biology requires a sophisticated understanding of how environmental  
471 stimuli affect the form and function of plants as well as an understanding of how physiological  
472 context informs such responses. Environmental conditions are at least as complex as the  
473 plants they affect. Plant roots are exposed to a variety of environmental signals that change  
474 in time and space at very different scales that are integrated at the whole plant system. It is  
475 an important challenge in biology to develop methods of growing and studying plants that  
476 present such stimuli in a manner that the plant is likely to encounter in nature. After all, the  
477 plants we study have evolved to survive through mechanisms that have been selected, over  
478 evolutionary time, in nature. It will be interesting for future studies to determine how other  
479 environmental stimuli affect root growth using GLO-Roots and whether these responses  
480 differ between accessions of Arabidopsis. Identification of the genetic loci responsible for  
481 phenotypic variation in adult root phenotypes may identify the molecular basis for adaptive  
482 variation that exists in this species and potentially identify loci that are useful for breeding

483 efforts needed for the next green revolution.

484 **Materials and methods**

485 **Growth system**

486 **Rhizotrons and growth system fabrication.** Rhizotrons are composed of two sheets of  
487 1/8" abrasion resistant polycarbonate plastic (Makrolon AR (R)) cut to size using a water  
488 jet (AquaJet LLC, Salem, OR), two acrylic spacers cut using a laser (Stanford Product  
489 Realization Lab), two rubber U-channels cut to strips 30 cm long ([McMaster Carr part](#)  
490 [# 8507K33](#)) and two sheets of black 0.030" thick polypropylene sheets ([McMaster Carr](#)  
491 [part # 1451T21](#)) cut with a straight-edge razor blade. Rhizotron designs were drafted in  
492 Adobe Illustrator (Adobe, San José, CA). The blueprints of all the parts are provided in  
493 Supplement 1. The top edge of each polycarbonate sheet was painted with black 270 Stiletto  
494 nail polish (Revlon, New York, NY).

495 **Boxes and holders.** Rhizotrons are held vertical during plant growth in a custom rack sys-  
496 tem composed of two sheets of 1/4" black acrylic plastic cut with slots for eleven rhizotrons  
497 using a laser, four 3/8" PVC rods ([McMaster Carr part # 98871a041](#)) secured with PVC  
498 nuts ([McMaster Carr part # 94806a031](#)) to hold the acrylic sheets horizontal. The rack is  
499 placed inside a 12" x 12" x 12" black polyethylene tank ([Plastic Mart part # R121212A](#)).

500 **Rhizotron preparation** The procedure to construct a rhizotron with soil is as follows:  
501 Two pieces of polycarbonate plastic are laid flat on a table with the spacers inserted. Using  
502 an electric paint gun, a fine mist of water is applied to the bare polycarbonate sheets. Then,  
503 using a 2 mm sieve (US Standard Sieve Series N° 10) a fine layer of PRO-MIX(r) PGX soil  
504 (Premier Tech, Canada) is applied. Excess soil is discarded by gently tapping the plastic  
505 against the table in a vertical position. Water is sprayed again onto the soil, then a second  
506 layer of Pro-MIX is applied as before. For P deficiency experiments soil supplemented with  
507 1 ml of 100 µM P-Alumina (control) and 0-P-Alumina (P deficient ) was used. To prevent  
508 the soil from falling out of the bottom opening, a 3 x 6 cm piece of nylon mesh is rolled into

509 a 1 cm wide tube and placed at the bottom side of the rhizotron. The spacers are removed  
510 and replaced by clean spacers. The two faces of the rhizotron are carefully joined together  
511 and two rubber U-channels slipped on to clamp all pieces together. Assembled rhizotrons  
512 are placed into the rack inside the boxes and 500 mL of water is added to the box.

513 **Plant growth** *Arabidopsis thaliana* seeds were stratified for 2 d at 4 °C in Eppendorf tubes  
514 with distilled water. Seeds were suspended in 0.1 % agar and 5 to 10 were sown using  
515 a transfer pipette in the rhizotron. A transparent acrylic sheet was mounted on top of  
516 the box and sealed with tape to ensure high humidity conditions that enable *Arabidopsis*  
517 germination. Three days after sowing, the cover was unsealed to decrease humidity and  
518 allow the seedlings to acclimate to a dryer environment. From 3 days after sowing (DAS)  
519 to the time the first true leaves emerged, it was critical to ensure that the top part of the  
520 rhizotron remained humid for proper germination of the plants. Between three and five DAS  
521 the rhizotrons were thinned leaving only the number plants required for that experiment,  
522 typically one, except for experiments examining root-root interactions. Unless otherwise  
523 stated, all the experiments presented here, treatments were started 10 DAS. Plants were  
524 grown under long day conditions (16 h light / 8 h dark) using 20–22 °C (day/night) and  
525 150 µE m<sup>-1</sup> s<sup>-1</sup>. Two types of growth environments were used for experiments. A walk-in  
526 growth chamber with fluorescent lightning and a growth cabinet with white LED lights.  
527 Relative water content measurements were done as previously described<sup>33</sup>

528 **qRT-PCR analysis.**

529 Seeds were surface sterilized as described before<sup>2</sup> and grown in rhizotrons, 100 cm<sup>3</sup> pots, or  
530 on two types of 1% agar (Duchefa) media containing either 1x MS nutrients (Caisson) and 1%  
531 Sucrose, (termed ms media) or 1/4x MS nutrients only (termed ms25 media). Both media were  
532 buffered using 0.5 g/L MES and pH was adjusted to 5.7 with KOH. All plants were grown  
533 together in a growth cabinet with LED lights under long day conditions (16h day/8h night).  
534 Root and shoot tissue was collected separately from individual plants at the end of the day  
535 (1 hour before the lights shut off) and at the end of the night (1 hour before lights came on).

536 Three biological replicates were collected for each condition. RNA was extracted using the  
537 Plant RNA MiniPrepTM kit (ZYMO Research) according to manufacturer's instructions  
538 with on-column DNase treatment (Qiagen). cDNA was made using the iScript Advanced  
539 cDNA Synthesis for RT-qPCR kit (Bio-Rad) from 200 ng of total RNA. qRT-PCR was  
540 performed using a Fluidigm BioMarkTM 96.96 Dynamic Array IFC with the EvaGreen®  
541 (Bio-Rad) fluorescence probe according to the Fluidigm Advanced Development Protocol  
542 number 37. For the analysis, all the reactions with no amplification ( $C_t = 999$ ) were set to  
543 the maximal  $C_t$  for that assay type. The two technical replicates were then averaged and  
544  $dC_t$  values calculated using AT3G07480, AT4G37830, At1g13320 and At1g13440 as reference  
545 internal controls. PCA plots were generated with Devium Web<sup>34</sup> using  $dC_t$  values.  $dCT$   
546 values were calculated as  $dCT = CT_{\text{gene interest}} - \text{mean}(CT_{\text{reference gene}})$ . Primers  
547 used are listed in file Supplement 8.

548 **Biological components**

549 **Codon optimization of luciferases.** The following luciferases that emit light at different  
550 wavelengths were codon optimized for Arabidopsis (Genscript, Piscataway, NJ): LUC2: a  
551 yellow improved version (Promega, Madison, WI) of the original *Photinus pyralis* (firefly)  
552 LUC.

- 553 • Ppy RE8: a red variant<sup>35</sup> of the *P. pyralis* thermostable variant Ppy RE-TS<sup>36</sup>.
- 554 • CBG99: a green variant (Promega, Madison, WI) from yellow click beetle (*Pyrophorus*  
555 *plagiophthalmus*) luciferases.
- 556 • CBR: a red variant (Promega, Madison, WI) from yellow click beetle.

557 **Non-optimized luciferases.** We also used the following non-optimized luciferases:

- 558 • nanoLUC: a blue luciferase isolated from a deep sea shrimp<sup>14</sup>.

- 559     • venusLUC2: a venus-LUC2 fusion reported to show higher luminescence output than  
560     LUC2<sup>12</sup>.
- 561     • A transposon containing the bacterial luciferase-containing LUX operon was inte-  
562     grated into the *Pseudomonas fluorescens* CH267<sup>19</sup> genome by conjugation with *E.*  
563     *coli* *SM10 pir* containing pUT-EM7-LUX<sup>37</sup> and used to track root microbe coloniza-  
564     tion. For inoculation 9 DAS plants were inoculated with 2 mL of an overnight bacterial  
565     culture resuspended in 10 mM MgSO<sub>4</sub> and diluted to 0.01 OD.

566 **Generation of single-reporter transgenic plants.** We generated transcriptional fu-  
567     sions of all luciferases to constitutive promoters to examine the activity level and emission  
568     spectrum of each isoform. The *attL1-attL2* entry clones containing plant-codon optimized  
569     coding sequence of *LUC2*, *PpyRe8*, *CBG99* and *CBR* were synthesized by Genscript. A  
570     DNA fragment including the *UBQ10* promoter region and first intron was amplified from  
571     Col-0 genomic DNA with primers incorporating the attB1, attB4 combination sites at the 5'  
572     and 3' respectively. The PCR product was then introduced into pDONR™ P4-P1R (Invitro-  
573     gen) through a classic Gateway BP-reaction. The resulting plasmid, the *attL1-attL2* entry  
574     clones with luciferase sequences, an empty *attR2-attL3\** entry clone and the destination  
575     vector dpGreenmCherry<sup>2</sup> were used to construct *ProUBQ10:LUC2o*, *ProUBQ10:PpyRE8o*,  
576     *ProUBQ10:CBG99o* and *ProUBQ10:CBRo* through Gateway LR reactions. The destination  
577     vector *dpGreenmCherry* contains a plasma membrane-localized mCherry coding sequence  
578     driven by the 35S promoter and is used as a selectable marker of transformation at the  
579     mature seed stage<sup>2</sup>. We used Golden Gate cloning and the destination vectors that we had  
580     generated before<sup>13</sup> for the following fusions: *ProUBQ10:nanoLUC2*, *ProUBQ10:venusLUC*,  
581     *ProACT2:PpyRE8o*. Briefly, the different components of each construct were PCR ampli-  
582     fied with complementary BsaI or SapI cutting sites, mixed with the destination vector in  
583     a single tube, digested with either BsaI or SapI, ligated with T4 DNA ligase, then trans-  
584     formed into *E. coli* Top10 cells and plated on LB antibiotic plates containing X-gal as pre-  
585     viously described<sup>13</sup>. Junction sites were confirmed by sequencing. We used pSE7 (Addgene  
586     ID #: pGoldenGate-SE7: 47676) as the destination vector of the *ProUBQ10:nanoLUC2*,

587 *ProUBQ10:venusLUC* constructs and pMYC2 (Addgene ID #: pGoldenGate-MCY2: 47679)  
588 as the destination vector for *ProACT2:PpyRE8o*. Maps of all the vectors can be found in  
589 Supplement 8. *ProUBQ10:LUC2o* was transformed into Col-0, Bay and Sha accessions, the  
590 *tir1-1*<sup>38</sup> mutant and the *miz1*<sup>39</sup> T-DNA insertion line (SALK\_126928).

591 **Brachypodium distachyon** The Arabidopsis plant-codon optimized Luciferase gene,  
592 *LUC2o*, was inserted into the monocot vector pANIC10 via Gateway cloning<sup>28</sup>. *Brachy-*  
593 *podium distachyon* plants were transformed using the method of Vogel and Hill<sup>40</sup>.

594 **Tomato** The transcriptional fusion *ProeDR5:LUC2* was generated by cloning the  
595 *ProeDR5:LUC2* DNA fragment into the pBIB expression vector via restriction sites SalI  
596 and Acc65I. The eDR5 promoter is an enhanced version of DR5 containing 13 repeats of  
597 the 11-nucleotide core DR5 element<sup>41</sup> and the pBIB expression vector contains an NPTII  
598 resistance gene under the control of the NOS promoter for use as a selectable marker during  
599 transformation. All tomato transformations were performed by the Ralph M. Parsons  
600 Foundation Plant Transformation Facility (University of California, Davis).

601 **Generation of dual-reporter plants.** To generate dual-reporter plants expressing lu-  
602 ciferase isoforms that emit light with divergent emission spectra we used *ProACT2:PpyRE8o*  
603 as the root structural marker and ZAT12:LUC<sup>18</sup> and DR5:LUC+<sup>17</sup> lines that were trans-  
604 formed with the *ProACT2:PpyRE8o* construct. All constructs were transformed using a  
605 modified floral dip method as described in<sup>2</sup>.

606 To make the dual color tomato plants, the *Pro35S:PpyRE8o* transcriptional fusion was  
607 generated by putting the plant-codon optimized coding sequence described above into the  
608 pMDC32 expression vector through a Gateway LR reaction. The pMDC32 vector con-  
609 tains a hygromycin resistance gene under the control of the 35S promoter for use as a se-  
610 lectable marker during transformation. This construct was transformed into the transgenic  
611 *ProeDR5:LUC2* tomato line.

612   **In vivo emission spectra of plants constitutively expressing luciferase isoforms.**

613   To generate *in vivo* emission spectra of all constitutively expressed luciferases, seeds were  
614   sterilized and sown on MS plates as described before<sup>2</sup>. After 8 days, seedlings were treated  
615   with a 100 µM luciferin solution, incubated at room temperature for 3 hours and imaged  
616   using an IVIS Spectrum imaging system (Perkin Elmer, Waltham , MA) using 20 nm band-  
617   pass emission filters at the following wavelengths (in nm: 490-510, 510-530, 530-550, 550-570,  
618   570-590, 590-610, 610-630, 630-650, 650-670, 670-690, 690-710). Raw images were analyzed  
619   using Fiji and *in vivo* emission spectra were constructed. The full emission spectra of LUX  
620   and nanoLUC could not be constructed since the maximum of these two luciferases is below  
621   the lower band pass filter that were available.

622   **Imaging system** We designed a custom imaging system (GLO1, Growth and Lumines-  
623   cence Observatory 1) optimized for imaging dual-reporter luciferase expression in our custom  
624   rhizotrons. The design was a joint effort with Bioimaging Solutions (San Diego, CA) who  
625   also built the system and wrote the acquisition software that drives all the mechanical parts  
626   of the system. The system is composed by two 2048 x 2048 PIXIS-XB cameras (Princeton  
627   Instruments, Trenton, NJ) mounted on top of each other to capture two fields of view en-  
628   compassing approximately two 15 x 15 cm areas corresponding to the top or bottom of the  
629   rhizotron. The cameras are fitted with a Carl-Zeiss macro lens. A filter wheel with space  
630   for four, 76.2 mm filters is positioned in front of the cameras and controlled by a stepper  
631   motor allowing for automated changing of the filter wheel position. We used two -542/50  
632   and 450/70- custom cut Brightline(R) band-pass filters (Semrock, Rochester, NY). In sin-  
633   gle color imaging mode, the filter wheel is operated without filters. Positioned in front of  
634   the filter wheel is a removable rhizotron holder mounted on a stepper motor. This stepper  
635   motor is also controlled by the GLO-1 software allowing automatic acquisition of images  
636   from both sides of the rhizotron sequentially. The whole imaging system is enclosed in a  
637   light-tight black box with a door that allows loading and un-loading of rhizotrons.

638 **Plant Imaging** Around 50 mL of 300  $\mu$ M D-luciferin (Biosynth, Itasca, IL) was added to  
639 soil at the top of the rhizotron. In general 5 min exposures were taken per rhizotron, per  
640 side, per channel. For daily imaging experiments, plants were imaged at dawn (+/- 1 hr)  
641 to reduce possible effects on diurnal rhythms of keeping plants in the dark during imaging.  
642 Shoot images were taken using a Nikon D3100 camera.

643 **Image Preparation** Four individual images are collected: top front, bottom front, top  
644 back and bottom back. Using an automated [ImageJ macro](#), a composite image is generated  
645 as follows: 1) To correct for differences in background values between the two cameras the  
646 mean background value of each image is subtracted from 200; 2) images are rotated and  
647 translated to control for small misalignments between the two cameras; 3) the top and  
648 bottom images of each side are merged; 4) the back image is flipped horizontally; 5) the  
649 front and back images are combined using the maximum values. When dual color images are  
650 acquired this operation is repeated for each channel. The final images produced are 16-bit  
651 depth and 4096 x 2048 pixels. The scale of the images is 138.6 pixels per cm. Considering  
652 that an Arabidopsis root is 100  $\mu$ m this results in 1.39 pixels across an Arabidopsis root.

653 **GLO-RIA imageJ plug-in** GLO-RIA uses a combination of existing tools to extract  
654 relevant root architecture features. Directionality is acquired using the [directionality plugin](#)  
655 from ImageJ. After the number of direction bins (we usually use bins of 2  $^{\circ}$ ) is defined by the  
656 user, a 5x5 sobel operator is used to derive the local gradient orientation. This orientation  
657 is then used to build a distribution of directions by assigning the square of the orientation  
658 into the appropriate bin. Instead of representing the total counts at each orientation a  
659 relative value is calculated by dividing the individual values at each bin by the total sum  
660 of the histogram (and multiplying by 100). Similar algorithms have been used to quantify  
661 dynamic changes in the plant cytoskeleton<sup>42</sup>.  
662 The Elliptic Fourier Descriptors are acquired using the [Fourier Shape Analysis plugin](#) on  
663 convex hull shape of the root system. Elliptic Fourier Descriptors have been used in numer-  
664 ous studies to analyse variations in shapes, notably in leaves (e.g<sup>43</sup>) The shape analysis is

665 inspired by RootScape<sup>15</sup>. Due to the absence of fixed, recognisable structures in root system  
666 (that are required for the position of true landmarks), pseudo-landmarks are automatically  
667 extracted from the root systems. Shortly, the image is divided vertically at equidistant posi-  
668 tions (with the number defined by the user) and for each of the image stripes, the minimum  
669 and maximum x coordinates are computed. The shape analysis is therefore able to discrim-  
670 inate root system with different vertical root distributions or global root system orientation  
671 (e.g. chemotropism) . The code source for the plugin, manual and sample images can be  
672 found in the [github repository](#) of the project.

673 Statistical analysis was performed in R<sup>45</sup>. The tidyR<sup>46</sup>, dplyr<sup>46</sup>, gridExtra<sup>47</sup>, shapes<sup>48</sup>,  
674 geomorph<sup>49</sup>, ggplot2<sup>50</sup> and cowplot<sup>51</sup> packages were used for data preparation, analysis  
675 and plotting. Final figure preparation was done in [Inkscape](#).

676 **Data availability** All the scripts and original data used to analyze and produce the  
677 images can be accessed in the Github repository of the project: [github.com/rr-lab/GLO-Roots](https://github.com/rr-lab/GLO-Roots). Raw files of all the images used in the paper are available in [Dryad](#).

## 679 Acknowledgements

680 Work in the lab of JRD was funded by the Carnegie Institution for Science Endowment  
681 and grants from the National Science Foundation (MCB-115795) and Department of En-  
682 ergy, Biological and Environmental Research program (DE-SC0008769). RRA was sup-  
683 ported by a Carnegie Postdoc Fellowship and currently by Conacyt Ciencia Básica Joven  
684 Investigador grant number (CB-2014-01-238101). GL was supported by the Belgian Fonds  
685 de la Recherche Scientifique. JM was funded by the National Science Foundation (IOS-  
686 0820854). CH is funded by MGH Toteston & Fund for Medical Discovery Fellowship grant  
687 2014A051303 and NIH R37 grant GM48707 and NSF grant MCB-0519898 awarded to Fred-  
688 erick Ausubel, and previously by the Gordon and Betty Moore Foundation through Grant  
689 GBMF 2550.01 from the Life Sciences Research Foundation. JV was funded by the Office  
690 of Biological and Environmental Research, Office of Science, US Department of Energy, in-

691 teragency agreements DE-SC0001526 and DE-AI02-07ER64452. We thank Robert Mittler  
692 and Philip Benfey for providing seeds of ZAT12:LUC and DR5:LUC+ respectively. We also  
693 thank Neil Robbins and members of the Dinneny lab for critical review of the manuscript  
694 and suggestions during the development of the project. We greatly appreciate Tim Doyle at  
695 the Stanford Small Animal Imaging Facility for providing's advice in using and help with  
696 luciferase-based imaging approaches.

697 **Competing interests**

698 We do not have any competing interests that we are aware of.

940    **References**

- 941    1.Dinneny, J. R. *et al.* Cell identity mediates the response of *Arabidopsis* roots to abiotic  
942    stress. *Science* **320**, 942–945 (2008).
- 943    2.Duan, L. *et al.* Endodermal ABA Signaling Promotes Lateral Root Quiescence during  
944    Salt Stress in Arabidopsis Seedlings. *Plant Cell* **25**, 324–341 (2013).
- 945    3.Lynch, J. P. & Wojciechowski, T. Opportunities and challenges in the subsoil: pathways  
946    to deeper rooted crops. *J. Exp. Bot.* **66**, 2199–2210 (2015).
- 947    4.Brady, N. C. & Weil, R. R. *Elements of the nature and properties of soils*. (Prentice Hall,  
948    2009).
- 949    5.Bao, Y. *et al.* Plant roots use a patterning mechanism to position lateral root branches  
950    toward available water. *Proc Natl Acad Sci* **111**, 9319–9324 (2014).
- 951    6.Tabata, R. *et al.* Perception of root-derived peptides by shoot LRR-RKs mediates systemic  
952    N-demand signaling. *Science* **346**, 343–346 (2014).
- 953    7.Rosquete, M. R. *et al.* An Auxin Transport Mechanism Restricts Positive Orthogravit-  
954    ropicism in Lateral Roots. *Current Biology* **23**, 817–822 (2013).
- 955    8.Uga, Y. *et al.* Control of root system architecture by DEEPER ROOTING 1 increases  
956    rice yield under drought conditions. *Nat. Genet.* **45**, 1097–1102 (2013).
- 957    9.Postma, J. A. & Lynch, J. P. The optimal lateral root branching density for maize depends  
958    on nitrogen and phosphorus availability. *Plant Physiol.* **166**, 590–602 (2014).
- 959    10.Schneider, C. A., Rasband, W. S. & Eliceiri, K. W. NIH Image to ImageJ: 25 years of  
960    image analysis. *Nature methods* **9**, 671–675 (2012).
- 961    11.Meijon, M., Satbhai, S. B., Tsuchimatsu, T. & Busch, W. Genome-wide association study  
962    using cellular traits identifies a new regulator of root development in. *Nat. Genet.* **46**, 77–81  
963    (2013).
- 964    12.Hara-Miyauchi, C. *et al.* Bioluminescent system for dynamic imaging of cell and animal  
965    behavior. *Biochem. Biophys. Res. Commun.* **419**, 188–193 (2012).

- 966 13.Emami, S., Yee, M.-C. & Dinneny, J. R. A robust family of Golden Gate Agrobacterium  
967 vectors for plant synthetic biology. *Front. Plant Sc.* **4**, 339 (2013).
- 968 14.Hall, M. P. *et al.* Engineered Luciferase Reporter from a Deep Sea Shrimp Utilizing a  
969 Novel Imidazopyrazinone Substrate. *ACS chemical biology* **7**, 1848–1857 (2012).
- 970 15.Ristova, D. *et al.* RootScape: a landmark-based system for rapid screening of root  
971 architecture in Arabidopsis. *Plant Physiology* **161**, 1086–1096 (2013).
- 972 16.Lobet, G. *et al.* Root System Markup Language: toward a unified root architecture  
973 description language. *Plant Physiol.* **167**, 617–627 (2015).
- 974 17.Moreno-Risueno, M. A. *et al.* Oscillating gene expression determines competence for  
975 periodic *Arabidopsis* root branching. *Science* **329**, 1306–1311 (2010).
- 976 18.Miller, G. *et al.* The plant NADPH oxidase RBOHD mediates rapid systemic signaling  
977 in response to diverse stimuli. *Science Signaling* **2**, ra45 (2009).
- 978 19.Haney, C. H., Samuel, B. S., Bush, J. & Ausubel, F. M. Associations with rhizosphere  
979 bacteria can confer an adaptive advantage to plants. *Nature Plants* **1**, 15051 (2015).
- 980 20.Mandoli, D. F., FORD, G. A., WALDRON, L. J., NEMSON, J. A. & Briggs, W. R. Some  
981 spectral properties of several soil types: implications for photomorphogenesis\*. *Plant Cell*  
982 *Environ.* **13**, 287–294 (1990).
- 983 21.Galen, C., Rabenold, J. J. & Liscum, E. Functional ecology of a blue light photoreceptor:  
984 effects of phototropin-1 on root growth enhance drought tolerance in *Arabidopsis thaliana*.  
985 *New Phytol.* **173**, 91–99 (2007).
- 986 22.Moni, A., Lee, A. Y., Briggs, W. R. & Han, I. S. The blue light receptor Phototropin 1  
987 suppresses lateral root growth by controlling cell elongation. *Plant Biology* 34–40 (2014).
- 988 23.Yokawa, K., Kagenishi, T. & Baluška, F. Root photomorphogenesis in laboratory-  
989 maintained *Arabidopsis* seedlings. *Trends Plant Sci.* **18**, 117–119 (2013).
- 990 24.Lobell, D. B. *et al.* Greater Sensitivity to Drought Accompanies Maize Yield Increase in  
991 the U.S. Midwest. *Science* **344**, 516–519 (2014).

- 992 25.Ort, D. R. & Long, S. P. Limits on Yields in the Corn Belt. *Science* **344**, 484–485 (2014).
- 993 26.Pacheco-Villalobos, D. & Hardtke, C. S. Natural genetic variation of root system archi-  
994 tecture from Arabidopsis to Brachypodium: towards adaptive value. *Philosophical Trans-  
995 actions of the Royal Society of London B: Biological Sciences* **367**, 1552–1558 (2012).
- 996 27.Watt, M., Schneebeli, K., Dong, P. & Wilson, I. W. The shoot and root growth of  
997 Brachypodium and its potential as a model for wheat and other cereal crops. *Functional  
998 Plant Biol.* **36**, 960–969 (2009).
- 999 28.Mann, D. G. J. *et al.* Gateway-compatible vectors for high-throughput gene functional  
1000 analysis in switchgrass (*Panicum virgatum L.*) and other monocot species. *Plant Biotechnol.  
1001 J.* **10**, 226–236 (2012).
- 1002 29.Pacheco-Villalobos, D., Sankar, M., Ljung, K. & Hardtke, C. S. Disturbed Local  
1003 Auxin Homeostasis Enhances Cellular Anisotropy and Reveals Alternative Wiring of  
1004 Auxin-ethylene Crosstalk in Brachypodium distachyon Seminal Roots. *PLoS Genet* **9**,  
1005 e1003564 (2013).
- 1006 30.Buer, C. S., Wasteneys, G. O. & Masle, J. Ethylene modulates root-wave responses in  
1007 Arabidopsis. *Plant Physiology* **132**, 1085–1096 (2003).
- 1008 31.Blossfeld, S., Schreiber, C. M., Liebsch, G., Kuhn, A. J. & Hinsinger, P. Quantitative  
1009 imaging of rhizosphere pH and CO<sub>2</sub> dynamics with planar optodes. *Annals of Botany* **112**,  
1010 267–276 (2013).
- 1011 32.Shaw, S. L. & Ehrhardt, D. W. Smaller, Faster, Brighter: Advances in Optical Imaging  
1012 of Living Plant Cells. *Annu. Rev. Plant Biol.* **64**, 351–375 (2013).
- 1013 33.Barr, H. & Weatherley, P. A re-examination of the relative turgidity technique for esti-  
1014 mating water deficit in leaves. *Aust. J. Biol. Sci* **15**, 413–428 (1962).
- 1015 34.Grapov, D. DeviumWeb: Dynamic Multivariate Data Analysis and Visualization Plat-  
1016 form.
- 1017 35.Branchini, B. R. *et al.* Red-emitting luciferases for bioluminescence reporter and imaging

- 1018 applications. *Analytical Biochemistry* **396**, 290–297 (2010).
- 1019 36.Branchini, B. R. *et al.* Thermostable red and green light-producing firefly luciferase  
1020 mutants for bioluminescent reporter applications. *Analytical Biochemistry* **361**, 253–262  
1021 (2007).
- 1022 37.Lane, M. C., Alteri, C. J., Smith, S. N. & Mobley, H. L. T. Expression of flagella is  
1023 coincident with uropathogenic Escherichia coli ascension to the upper urinary tract. *Proc.  
1024 Natl. Acad. Sci. U.S.A.* **104**, 16669–16674 (2007).
- 1025 38.Ruegger, M. *et al.* The TIR1 protein of Arabidopsis functions in auxin response and is  
1026 related to human SKP2 and yeast grr1p. *Genes Dev* **12**, 198–207 (1998).
- 1027 39.Moriwaki, T. *et al.* Hormonal Regulation of Lateral Root Development in Arabidopsis  
1028 Modulated by MIZ1 and Requirement of GNOM Activity for MIZ1 Function. *Plant Physiol.*  
1029 **157**, 1209–1220 (2011).
- 1030 40.Vogel, J. & Hill, T. High-efficiency Agrobacterium-mediated transformation of Brachy-  
1031 podium distachyon inbred line Bd21-3. *Plant Cell Rep* **27**, 471–478 (2008).
- 1032 41.Covington, M. F. & Harmer, S. L. The Circadian Clock Regulates Auxin Signaling and  
1033 Responses in Arabidopsis. *Plos Biol* **5**, e222 (2007).
- 1034 42.Lindeboom, J. J. *et al.* A Mechanism for Reorientation of Cortical Microtubule Arrays  
1035 Driven by Microtubule Severing. *Science* **342**, 1245533–1–1245533–11 (2013).
- 1036 43.Chitwood, D. H. *et al.* A modern ampelography: a genetic basis for leaf shape and  
1037 venation patterning in grape. *Plant Physiology* **164**, 259–272 (2014).
- 1038 44.Iwata, H. & Ukai, Y. SHAPE: a computer program package for quantitative evaluation of  
1039 biological shapes based on elliptic Fourier descriptors. *The Journal of Heredity* **93**, 384–385  
1040 (2002).
- 1041 45.R Core Team. *R: A language and environment for statistical computing*. (R Foundation  
1042 for Statistical Computing, 2014). at <<http://www.R-project.org/>>

- 1043 46.Wickham, H. *Tidyr: Easily tidy data with spread() and gather() functions.* (2014). at  
1044 <<http://CRAN.R-project.org/package=tidyr>>
- 1045 47.Auguie, B. *GridExtra: Functions in grid graphics.* (2012). at <<http://CRAN.R-project.org/package=gridExtra>>
- 1047 48.Dryden, I. L. *Shapes: Statistical shape analysis.* (2013). at <<http://CRAN.R-project.org/package=shapes>>
- 1049 49.Adams, D. & Otarola-Castillo, E. Geomorph: An r package for the collection and analysis  
1050 of geometric morphometric shape data. *Methods in Ecology and Evolution* **4**, 393–399 (2013).
- 1051 50.Wickham, H. *Ggplot2: Elegant graphics for data analysis.* (Springer New York, 2009).  
1052 at <<http://had.co.nz/ggplot2/book>>
- 1053 51.Wilke, C. O. *cowplot: Streamlined Plot Theme and Plot Annotations for ggplot2.* (2015).  
1054 at <<http://cran.r-project.org/web/packages/cowplot/index.html>>

<sub>699</sub> **Tables**

<sub>700</sub> **Table 1:** Luciferases used in this study.

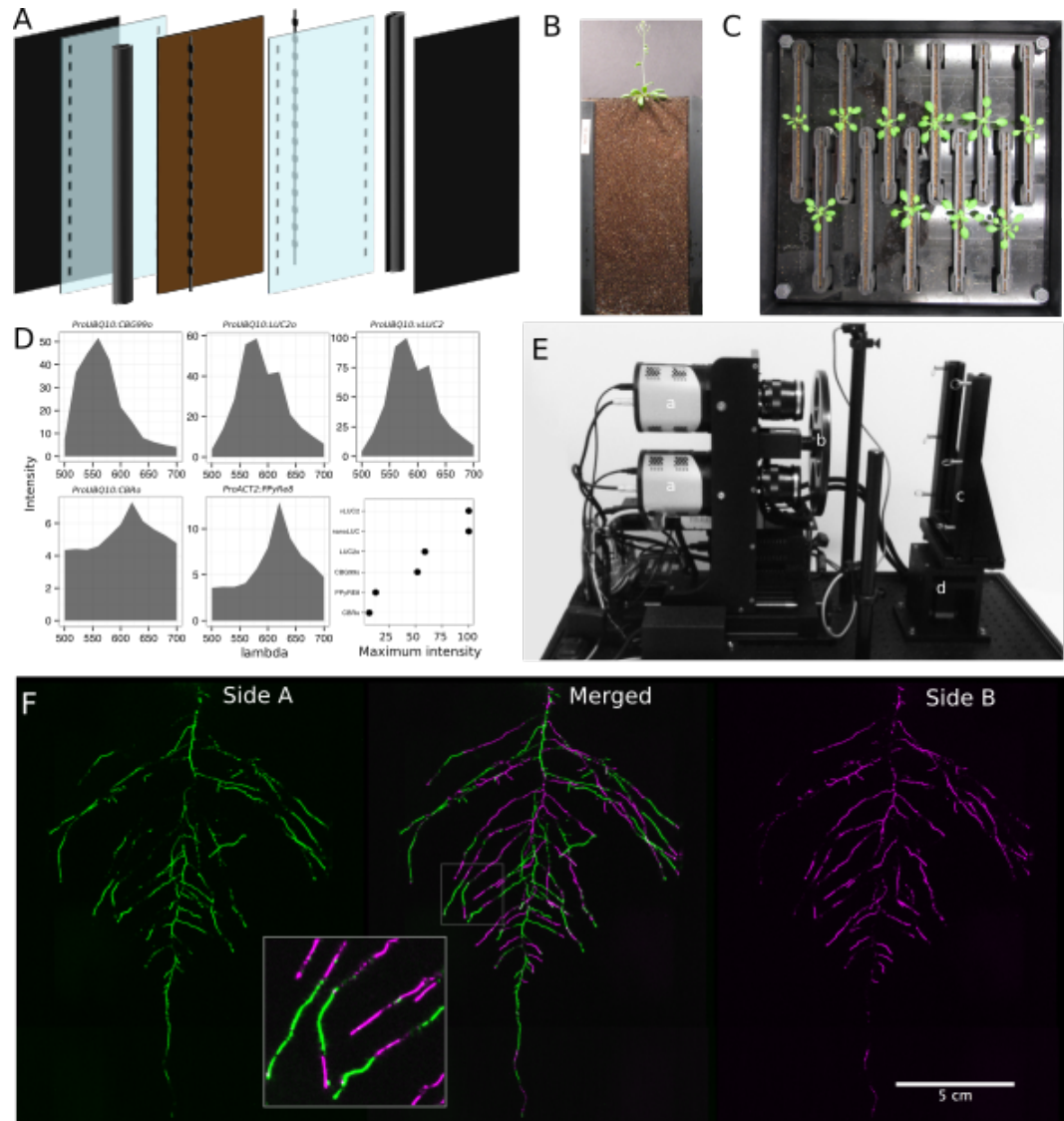
Luciferase	Origin	maximum wavelength	Substrate
Ppy RE8	firefly	618	D-luciferin
CBGRed	click beetle	615	D-luciferin
venus-LUC2	FP + firefly	580	D-luciferin
LUC(+)	firefly	578	D-luciferin
CBG99	click beetle	537	D-luciferin
lux operon	A. fischeri	490	biosynthesis pathway encoded within operon
nanoLUC	Deep sea shrimp	470	furimazine

<sub>701</sub> **Table 2:** list of root system features extracted using GLO-RIA.

variable	unit
projected area	cm <sup>2</sup>
number of visible roots	-
depth	cm
width	cm
convex hull area	cm <sup>2</sup>
width	cm
feret	cm
feret angle	°
circularity	-
roundness	-
solidity	-
center of mass	cm
Directionality	°
Euclidean Fourier Descriptors	-

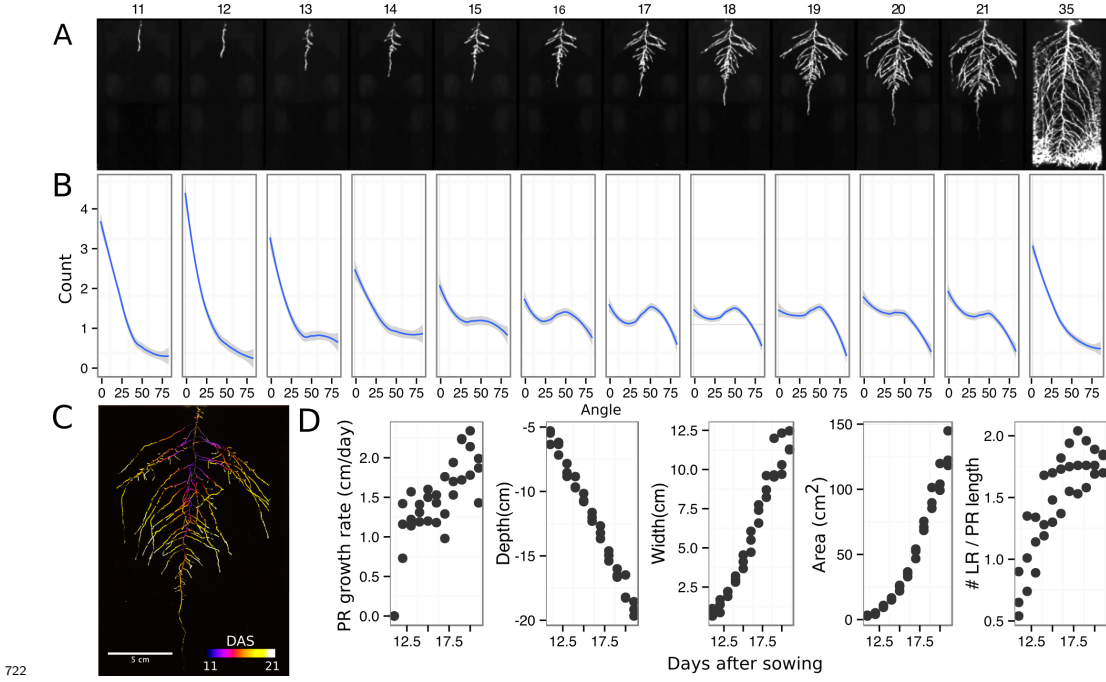
variable	unit
Pseudo landmarks	-

702 **Figures**

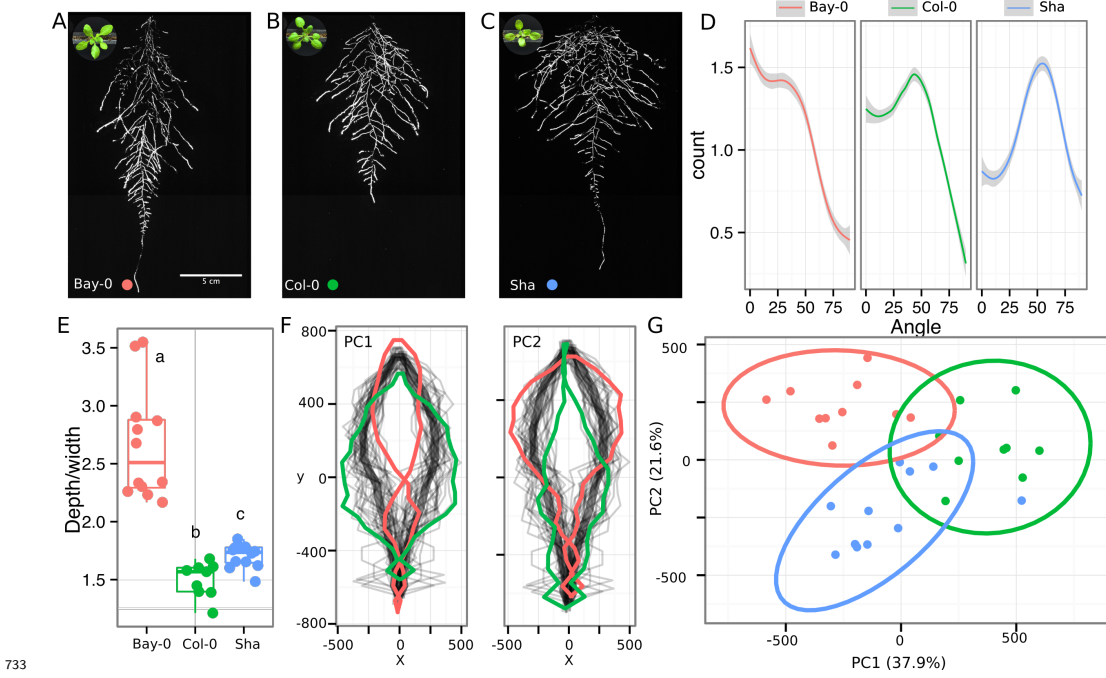


703  
 704 **Figure 1. GLO-Roots growth and imaging systems** A) 3D representation of the  
 705 different physical components of the rhizotron: plastic covers, polycarbonate sheets,  
 706 spacers and rubber U-channels. Blueprints are provided in Supplementary material 1. In brown,  
 707 soil layer. B) Thirty five day-old plant in rhizotron with black covers removed. C) Top view  
 708 of holding box with eleven rhizotrons. D)In vivo emission spectra of different luciferases  
 709 used in this study. Transgenic homozygous lines expressing the indicated transgenes were

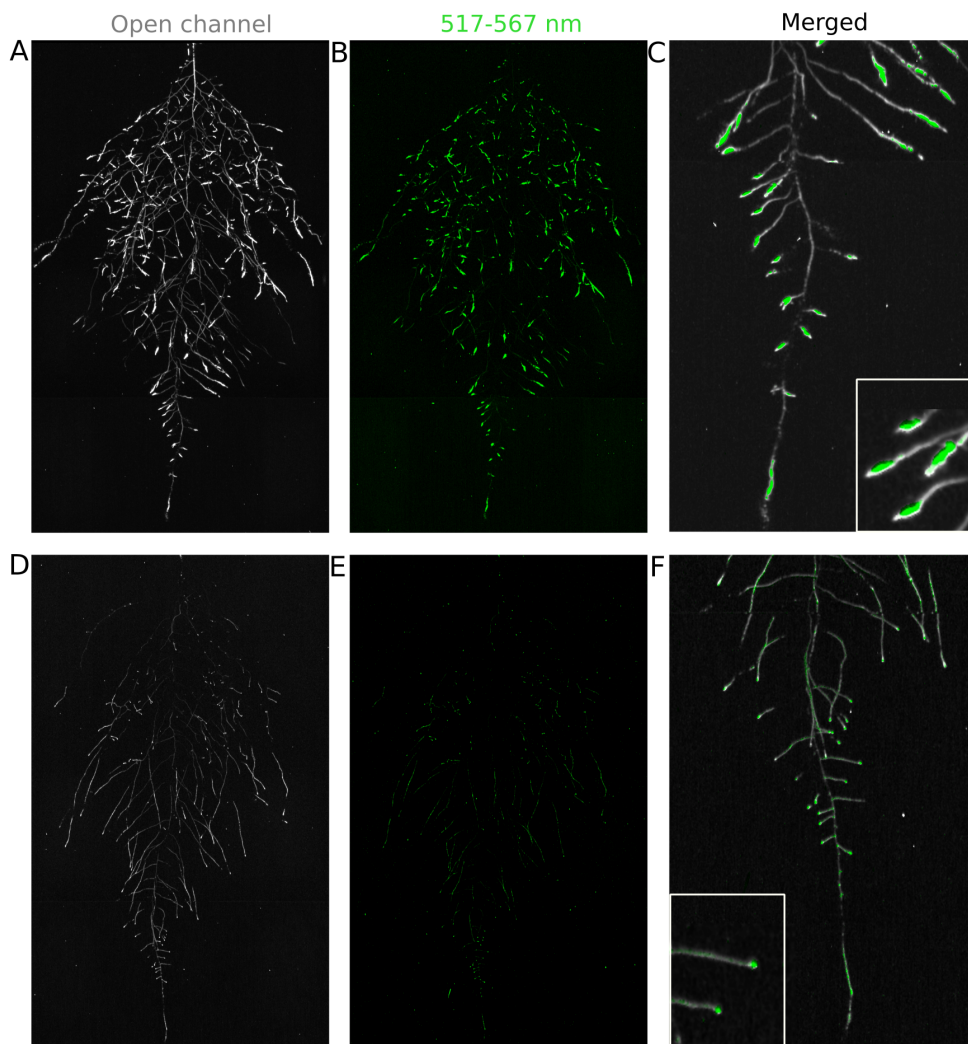
710 grown on agar media for 8 days. Luciferin (300  $\mu$ M) was sprayed on the seedlings and  
711 plates were kept in the dark and then imaged for 2 s at wavelengths ranging from 500  
712 to 700 nm. Five intensity values were taken from different parts of the roots of different  
713 seedlings and averaged. Relative maximum intensity values are indicated in the lower right  
714 graph. E) GLO 1 imaging system. The system is composed by two back illuminated CCD  
715 cameras (a) cooled down to -55 °C. A filter wheel (b) allows for spectral separation of the  
716 different luciferases. On the right, a rhizotron holder (c) is used to position the rhizotrons  
717 in front of the cameras. A stepper motor (d) rotates the rhizotron 180° to image both  
718 sides. F) A 21 DAS plant expressing *ProUBQ10:LUC2o* was imaged on each of two sides  
719 of the rhizotron; luminescence signal is colorized in green or magenta to indicate side. In  
720 the middle of the panel, a combined image of the two sides is shown. The inset shows a  
721 magnified part of the root system. FW: fresh weight, PR: Primary root.



723 **Figure 2. Time-lapse imaging of root systems and quantification using GLO-**  
 724 **RIA.** A) Typical daily time-lapse image series from 11 to 35 DAS of a *ProUBQ10:LUC2o*  
 725 Col-0 plant. B) Directionality of the root system of plants in panel A calculated using the  
 726 directionality plugin implemented in GLO-RIA. C) Color coded projection of root growth  
 727 using the images in panel A. D) Primary root growth rate, depth, width, root system area  
 728 are automatically calculated from the convex hull, which is semi-automatically determined  
 729 with GLO-RIA. Lateral root number and number of lateral roots divided by the primary  
 730 root length were quantified manually. A Local Polynomial Regression Fitting with 95%  
 731 confidence interval (grey) was used to represent the directionality distribution curve. ( $0^\circ$  is  
 732 the direction of the gravity vector).



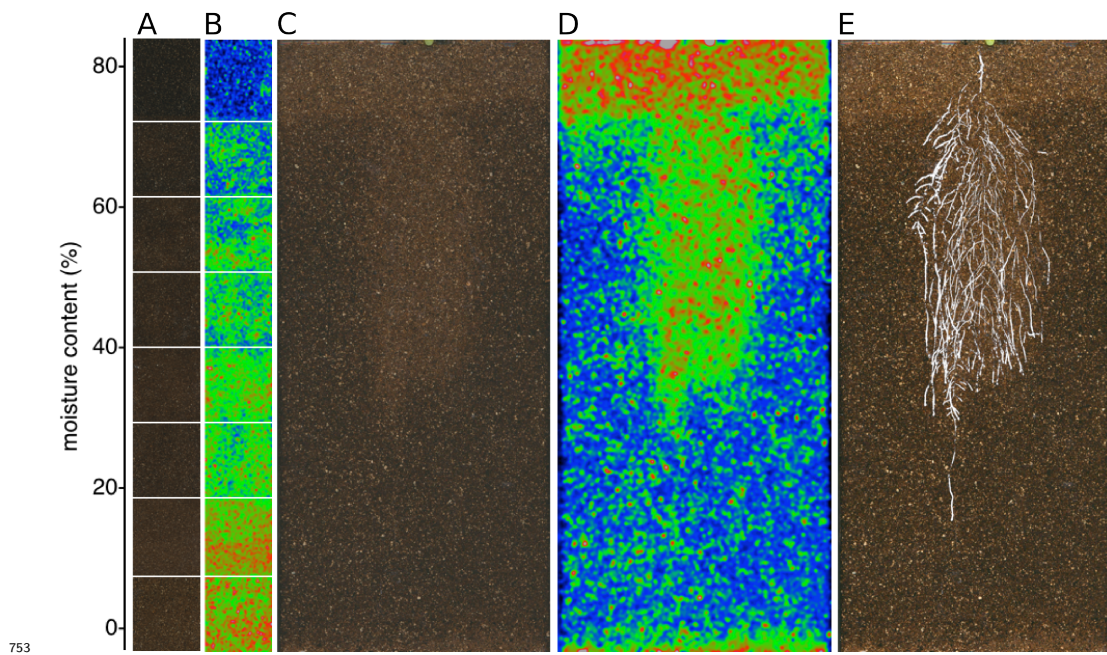
734 **Figure 3. Variation in root architecture between accessions of *Arabidopsis*.** Rep-  
 735 resentative root and shoot images of A) Bay-0, B) Col-0 and C) Sha accessions transformed  
 736 with *\_ProUBQ10:LUC2o\_* and imaged after 22 DAS. D) Directionality of the root systems,  
 737 E) depth/width ratio, F) Pseudo-landmarks describing shape variation in root system archi-  
 738 tecture. Eigenvalues derived from the analysis of 9-12 plants per accession is shown. The  
 739 first two Principal Components explaining 38% (PC1) and 22% (PC2) of the shape variation  
 740 are plotted. PC1 captures homogeneity of root system width along the vertical axis and  
 741 PC2 a combination of depth and width in top parts of the root system. Red and green  
 742 lines indicate -3SD and +3SD (Standard Deviations), respectively G) PC separation of the  
 743 different ecotypes using the PCs described in (F). A Local Polynomial Regression Fitting  
 744 with 95% confidence interval (grey) was used to represent the directionality distribution  
 745 curve. 0° is the direction of the gravity vector. Wilcoxon test analysis with p < 0.01 was  
 746 used to test significant differences between the different accession (n = 9-12 plants).



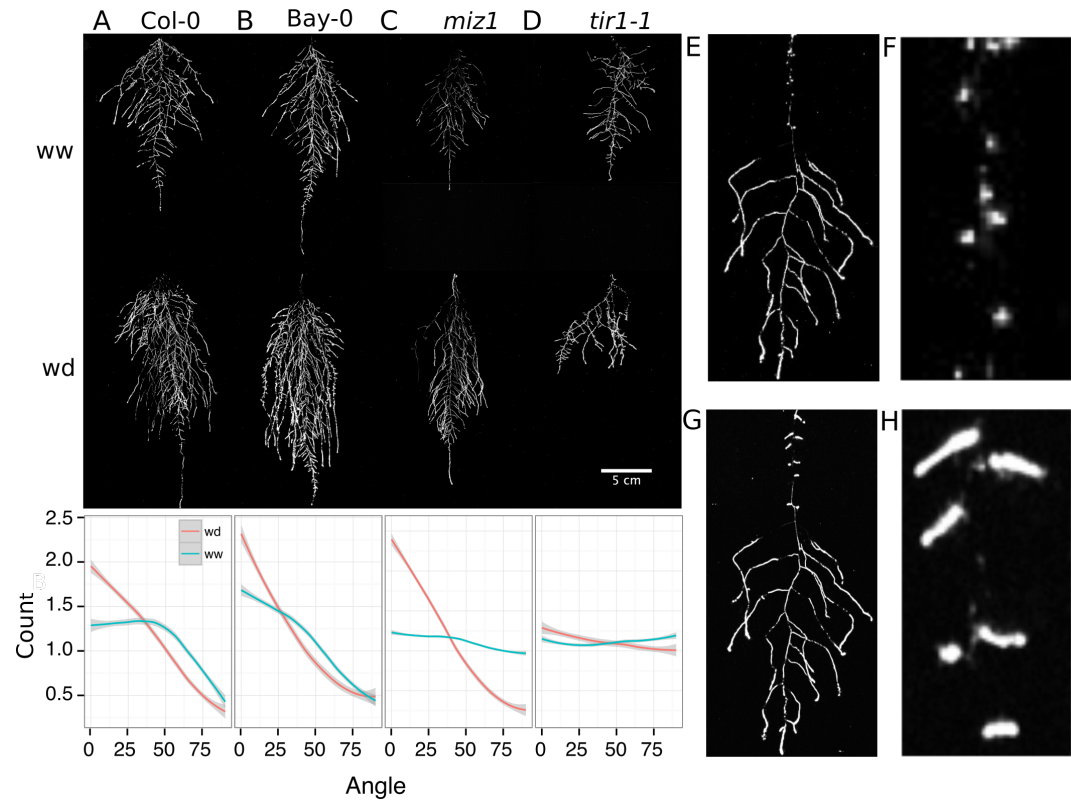
747

748 **Figure 4. Dual-color reporter visualization of structure and gene expression.**

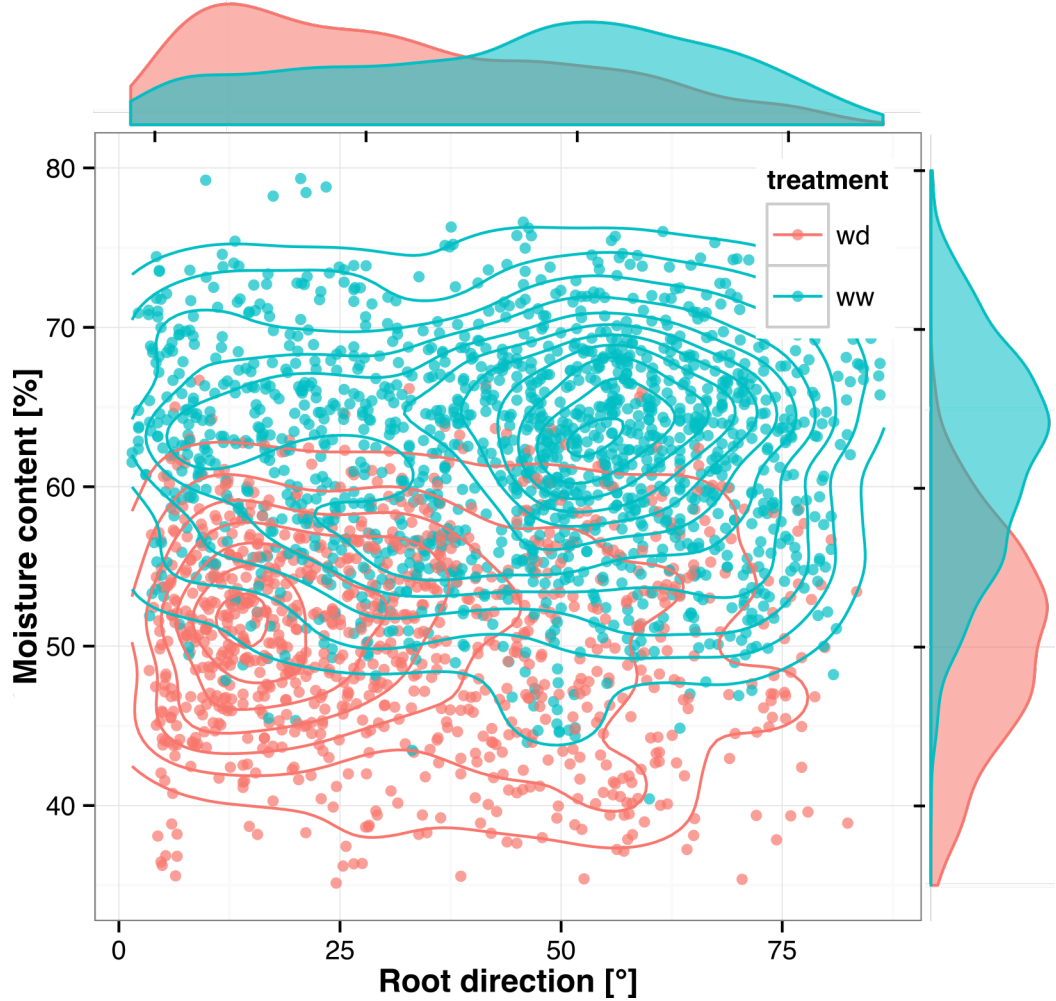
749 Images of whole root systems (A, D) or magnified portion of roots (C, F) at 22 DAS  
 750 expressing *ProDR5rev:LUC+* (green, A, B) or *ProZAT12:LUC* signal (green, D, E) with  
 751 skeletonized representation of roots generated using the *ProACT2:PpyRE8o* reporter  
 752 expression (in grey).



753     **Figure 5. Soil moisture and root architecture mapping in rhizotrons.** A) Com-  
 754     posite image showing regions of soil made from rhizotrons prepared with different moisture  
 755     levels. B) Differences in grey-scale intensity values were enhanced using a 16-color Look  
 756     Up Table (LUT). Brightfield image of soil in rhizotron (C) and converted using 16-color  
 757     LUT to enhance visualization of distribution of moisture (D) . E) Root system of a Bay-0  
 758     22 DAS and subjected to water deprivation since 13 DAS. Root system visualized using  
 759     luminescence and overlaid on brightfield image of soil in (C).  
 760

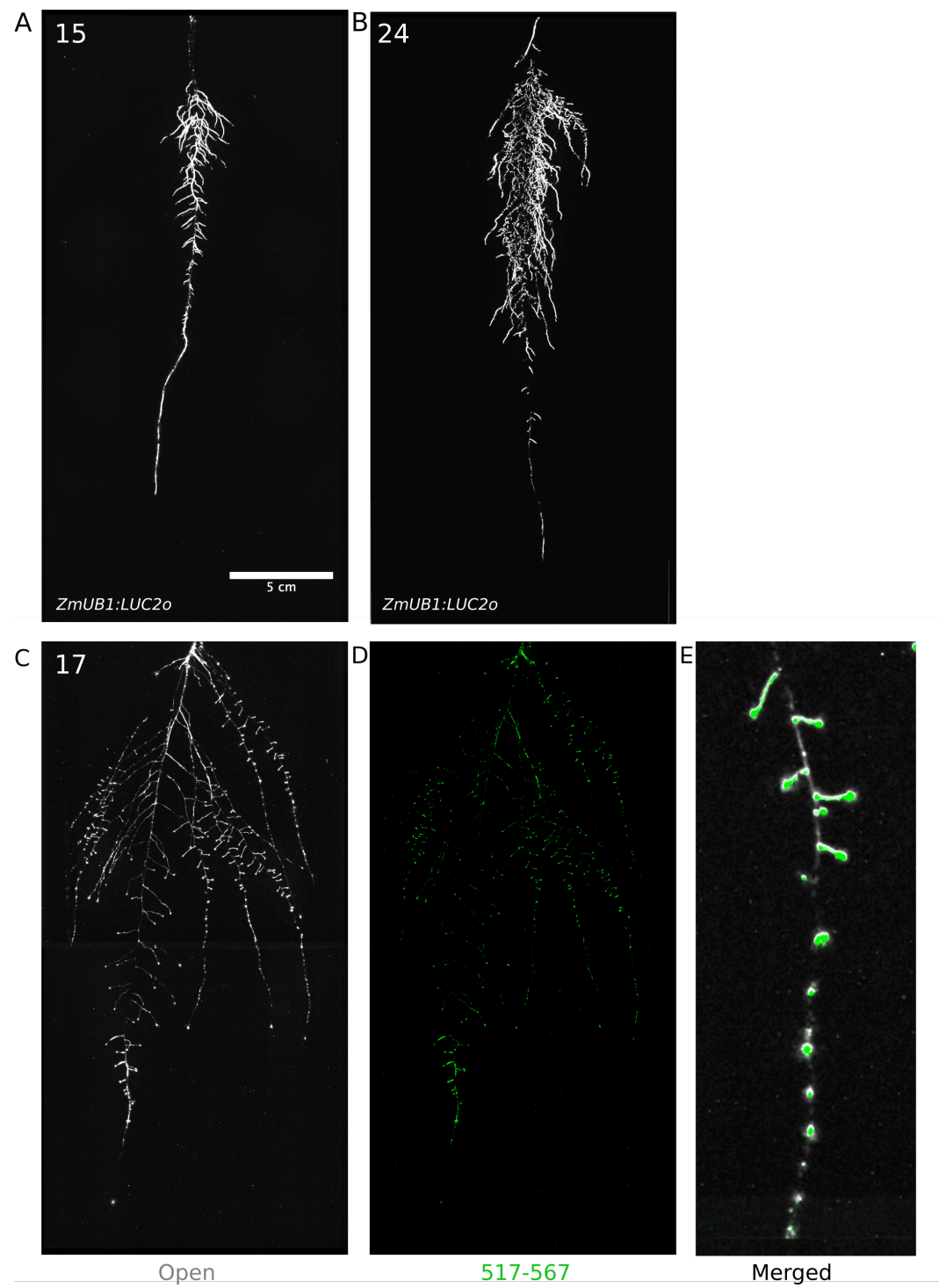


761  
 762 **Figure 6. Study of effect of water deficit on root system architecture.** A-D)  
 763 Root systems 22 DAS and exposed to water deficit 13 DAS onwards. Sample images of  
 764 well watered (left panels) and water deficit (right panels) root systems treated from 13  
 765 DAS and directionality (line graphs to left of images) for (A) Col-0 (B) Bay-0 (C) *miz1*  
 766 mutant and (D) *tir1-1*. E) Root system of a 22 DAS plant exposed to water deprivation  
 767 from 9 DAS onwards with magnified view of lateral root primordia (F). G) The same  
 768 root as in (E) 24 hours after rewatering and magnified view of lateral root primordia (H).  
 769 Kolmogorov-Smirnov test at  $p < 0.001$  was used to compare directionality distributions  
 770 between the different treatments and genotypes. A Local Polynomial Regression Fitting  
 771 with 95% confidence interval (grey) was used to represent the directionality distribution  
 772 curve.  $0^\circ$  is the direction of the gravity vector.



773

774 **Figure 7.** Relationship between local soil moisture content and root growth  
 775 direction. Data quantified from the time lapse series shown in [Video 2](#). Density plots  
 776 shown at periphery of graph for root direction (x-axis) and soil moisture (y-axis).  $0^\circ$  is  
 777 the direction of the gravity vector. Data represents 2535 root tips measured in a series  
 778 encompassing 10 time points.



779 **Figure 8:** Roots of *Brachypodium distachyon* transformed with *ProZmUB1:LUC2o* and

780

<sup>781</sup> imaged at 15 (A) and 24 (B) DAS grown in control conditions. C) Open channel of 17  
<sup>782</sup> DAS tomato plant transformed with *ProeDR5rev:LUC2o* and *Pro35S:PPyRE8o* D) Green  
<sup>783</sup> channel showing only *ProeDR5rev:LUC2o* E) Amplification of the open and green channel  
<sup>784</sup> showing increased expression of *ProeDR5rev:LUC2o* reporter in early-stage lateral roots.

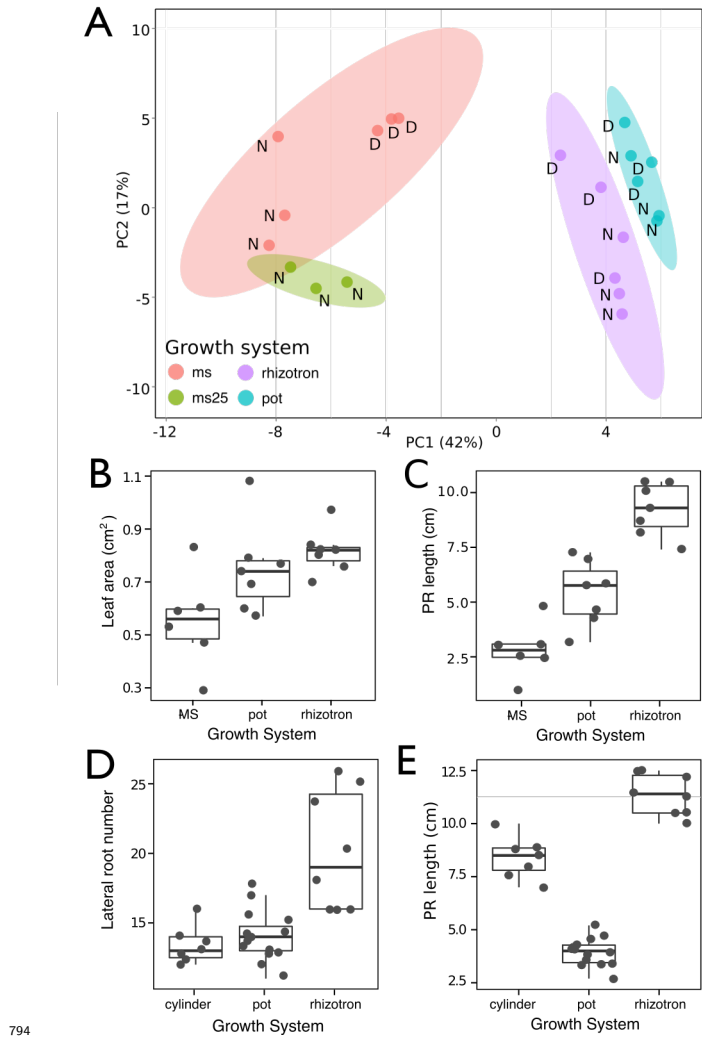
785    **Videos**

786    **Video 1** Time lapse from 11 to 21 DAS of a Col-0 plant expressing ProUBQ10:LUC2o  
787    grown in control conditions

788    **Video 2** Time lapse from 16 to 24 DAS of Col-0 plants expressing *ProUBQ10:LUC2o*  
789    growing in water deficient (left) and control (right) conditions. Plants were sown under  
790    control conditions and water deficit treatment started 11 DAS. Images were taken every  
791    day.

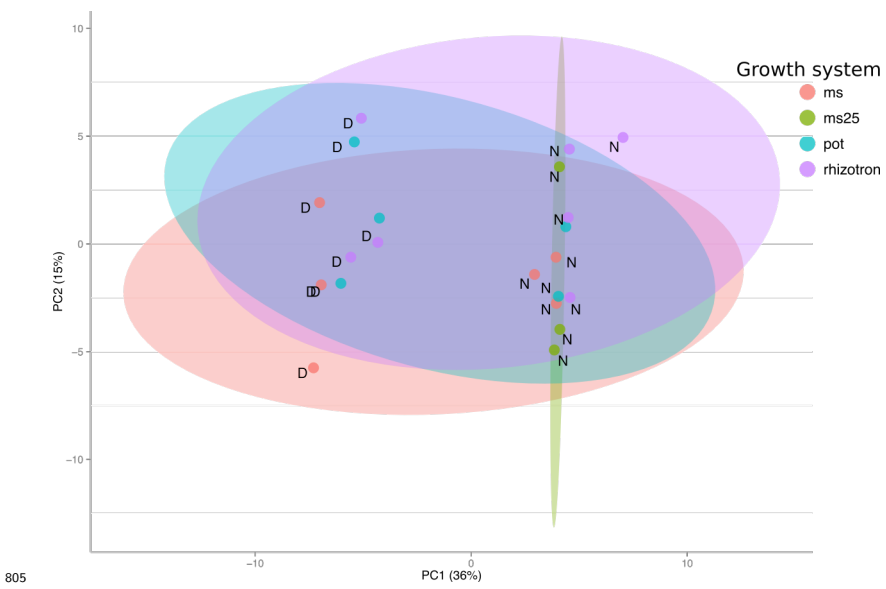
792    **Supplementary Material**

793    **Supplementary figures**



794    **Figure 1-figure supplement 1. Effect of different growth systems on plant biology.** A) Principal Components Analysis (PCA) score plot of a set of 76 genes analyzed by qPCR from root samples of plants grown in MS plates, pots, and rhizotrons. After 15 DAS three plants were collected at the end of the day (D) and three were collected at the end of the night (N). (ms = plant grown in full ms and 1% sucrose, ms25 = plants grown in 25% of full ms) B) Lateral root number and G) primary root length of 18 DAS plants grown in

<sup>801</sup> 30 cm tall cylinders, pots and rhizotrons, all with a volume of 100 cm<sup>3</sup> (n = 6-12 plants).  
<sup>802</sup> D) Leaf area and E) primary root length of plants of the same age (15 DAS) as the ones  
<sup>803</sup> used for the qPCR experiment (n= 6-7). ANOVA analysis with p < 0.01 was used to test  
<sup>804</sup> significant differences between the different parameters.

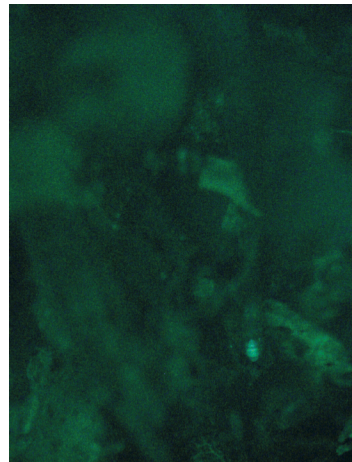


806 \*Figure 1-figure supplement 2. PCA plot of shoots of the same samples analyzed in Figure

807 1. See Figure 1 for more details regarding experimental conditions used.

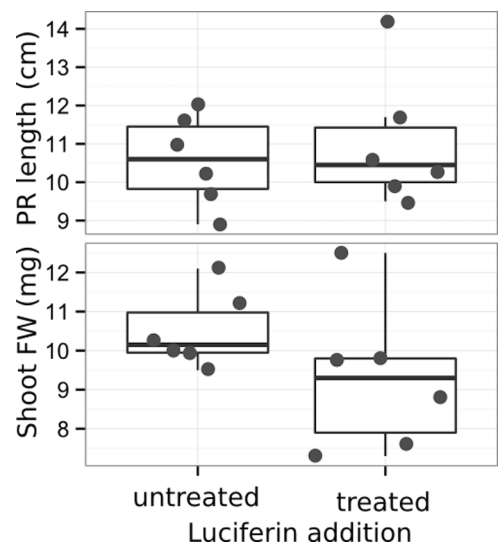


Brightfield  
808



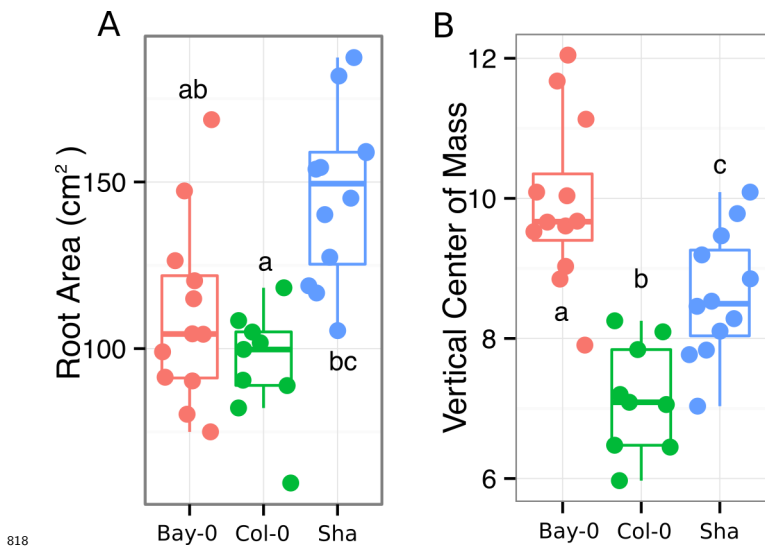
GFP

809 **Figure 1-figure supplement 3** Image of an Arabidopsis root in soil imaged with white  
810 light (brightfield) or epifluorescence.



811  
 812 **Figure 1-figure supplement 4** Effect of luciferin addition on primary root length and  
 813 shoot size of 14 DAS seedlings that were either continuously exposed to 300  $\mu$ M luciferin  
 814 from 9 DAS after sowing or not.

<sup>815</sup> **Figure 1-figure supplement data 1:** Two way ANOVA P-values comparing plants grown  
<sup>816</sup> in MS media vs. plants grown in soil (pots or rhizotrons) and plants collected at day or night.  
<sup>817</sup> We used p-value < 0.00065 threshold based on Bonferoni adjustment for multiple testing.



818    **Figure 3-figure supplement 1** A) root area, B) vertical center of mass of Bay-0, Col-0  
 819    and Sha accessions.  
 820

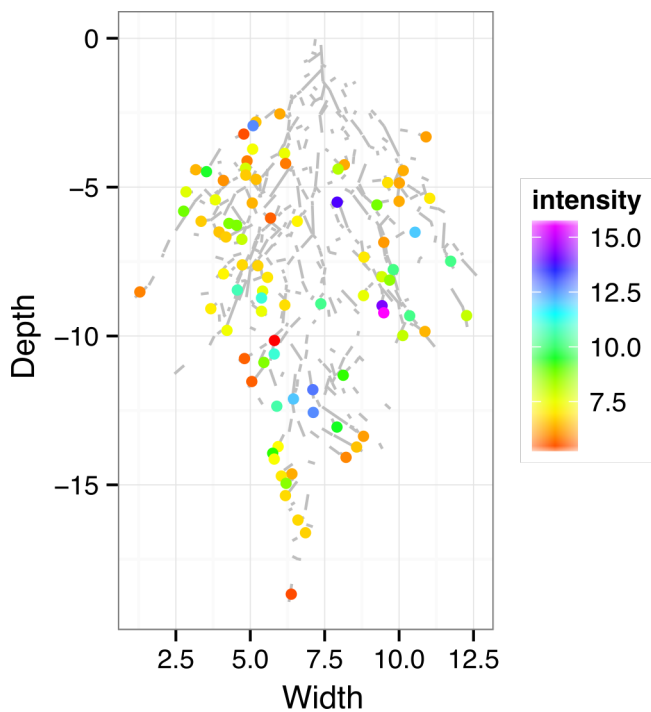
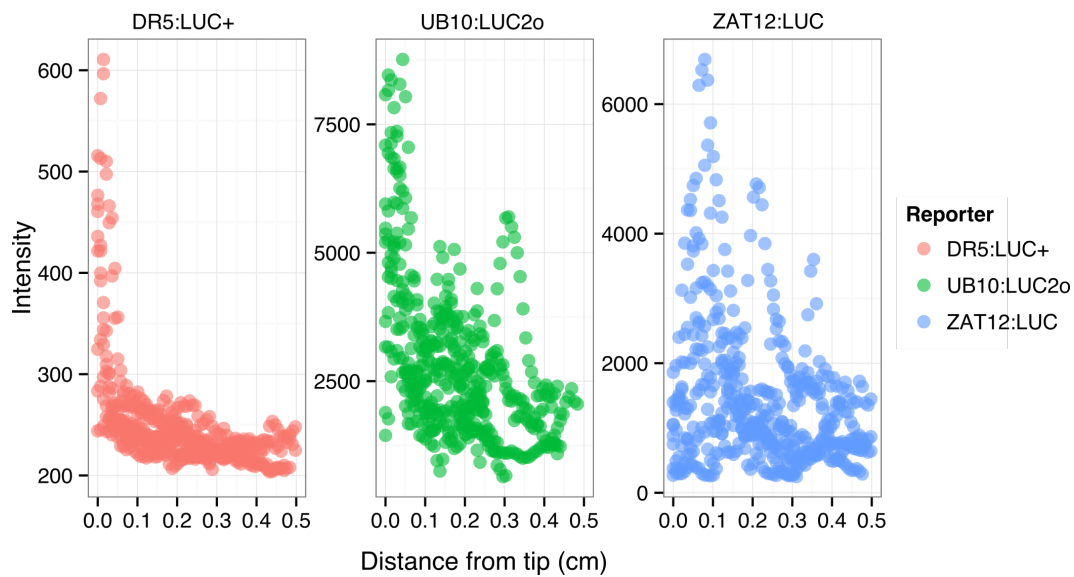


**Figure 4-figure supplement 1:**

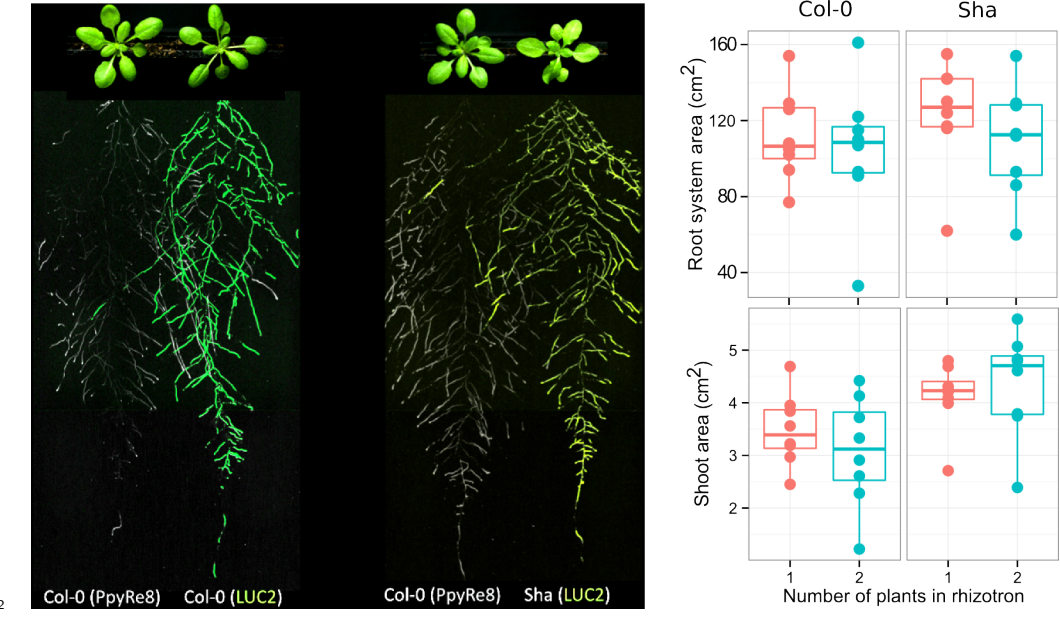
821  
 822 ZAT12:LUC intensity and root segments automatically identified values along the root tip.  
 823 Data was manually obtained by obtaining the intensity profile of the first 0.5 cm from the  
 824 root tip of individual lateral roots. Ten lateral roots for each reporter were measured.  
 825

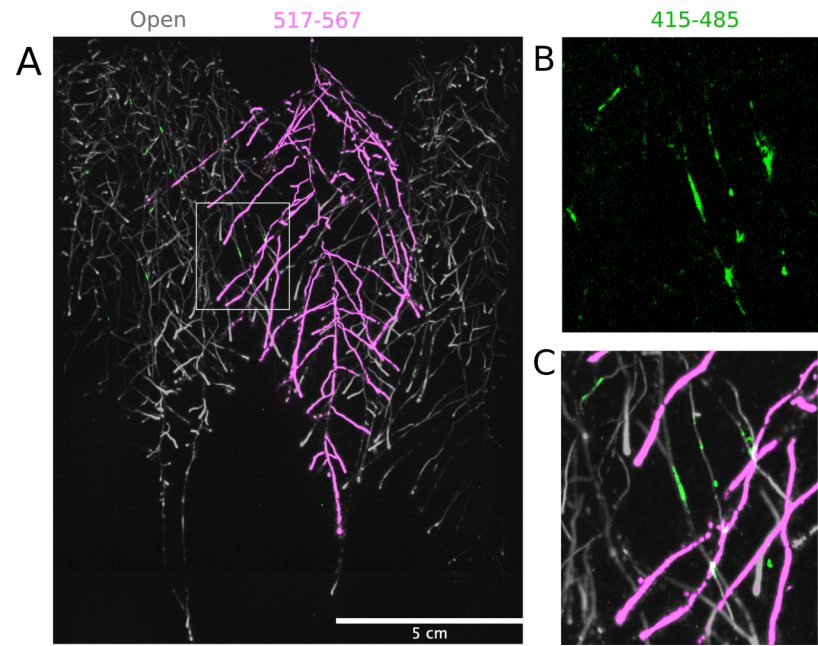


826

827 **Figure 4-figure supplement 2:** DR5:LUC+, UBQ10:LUC2o and ZAT12:LUC intensity  
 828 values along the root tip. Data was manually obtained by obtaining the intensity profile  
 829 of the first 0.5 cm from the root tip of individual lateral roots. Ten lateral roots for each  
 830 reporter were measured.

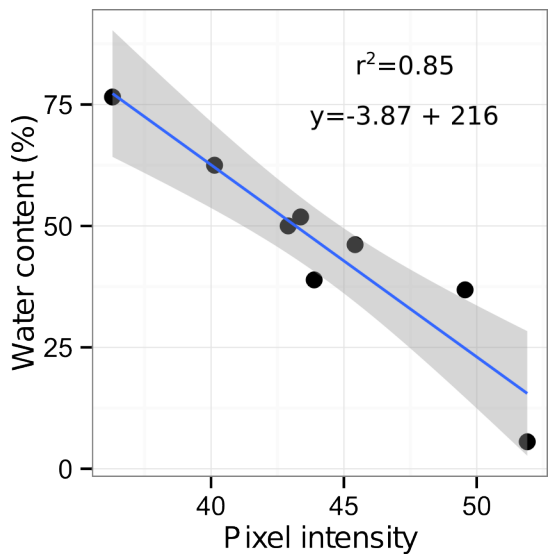
831





838      **Figure 4-figure supplement 4. Three-reporter-based analysis of root-root-  
 839      microbe interactions.** A) Image showing a 22 DAS *ProUBQ10:LUC2o* plant (magenta)  
 840      grown in the same rhizotron with *ProACT2:PpyRE8o* plants (grey). Plants were inoculated  
 841      with *Pseudomonas fluorescens* CH267 (green). Magnified portion of root systems colonized  
 842      by *Pseudomonas fluorescens* showing *P. fluorescences* (B) only or all three reporters  
 843      together (C).

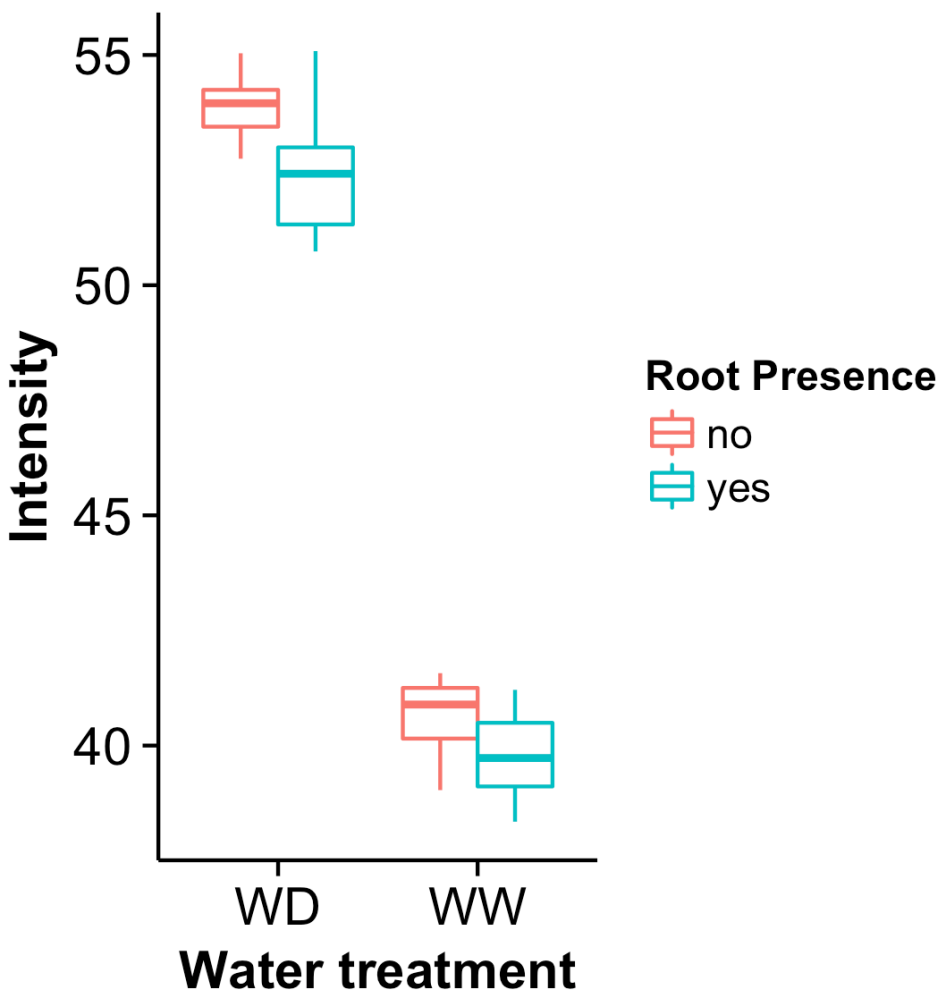
845



846

847 **Figure 5-figure supplement 1:** Moisture calibration curve. Rhizotrons with different  
848 levels of moisture were prepared and scanned to obtain readings of pixel intensity. Soil from  
849 rhizotrons was then weighed, dried down in an oven at 70 °C for 48 hours and percent water  
850 content quantified.

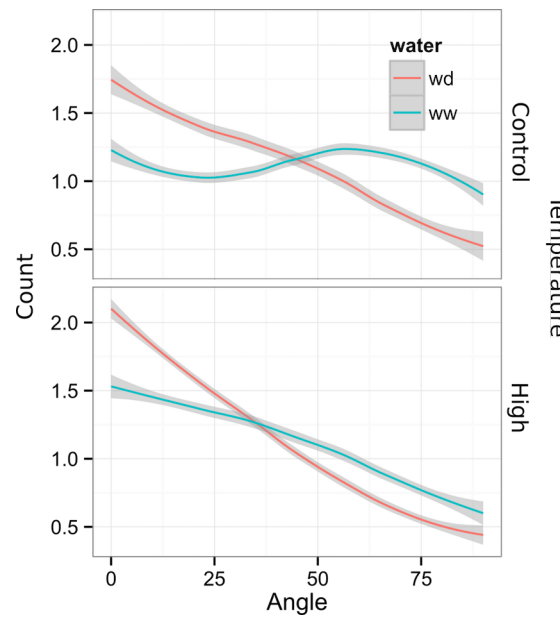
851



852

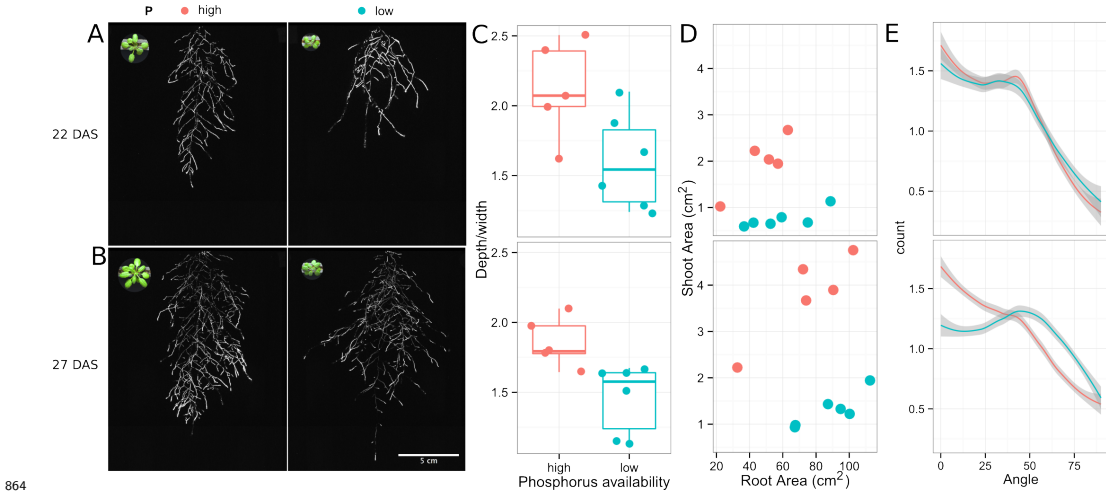
853 **Figure 5-figure supplement 2.** Comparison of soil intensity values between  
854 **areas of the rhizotron with or without the presence of roots, determined based**  
855 **on luminescence data.** Mean intensity values from 100 x 100 pixel squares samples of  
856 both areas were obtained from 10 different rhizotrons. Wilcoxon test analysis with  $p < 0.01$   
857 was used to test significant differences between areas with our without root presence.

858



859  
860 **Figure 6-figure supplement 1** Directionality analysis of roots of plants transferred to  
861 water deprivation conditions after 9 DAS and kept 22 °C (control temperature) and 29 °C  
862 (high temperature) until 22 DAS. (0° is the direction of the gravity vector).

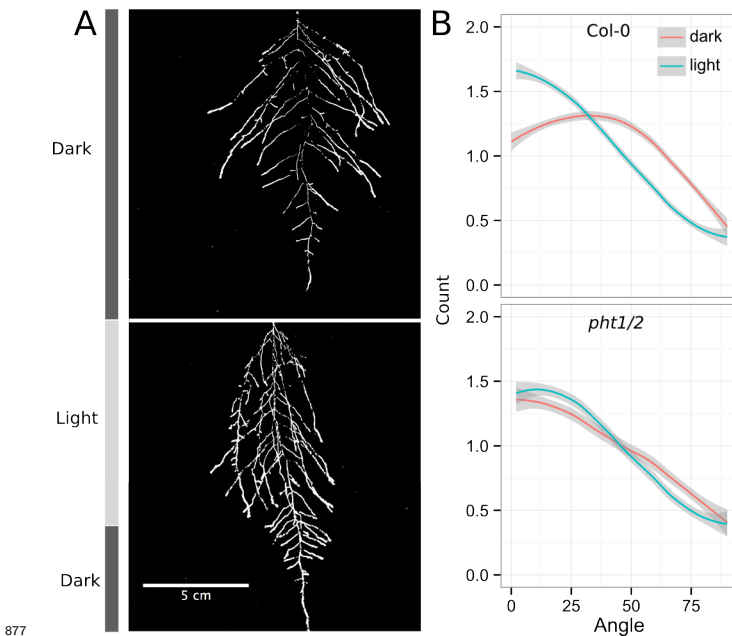
863



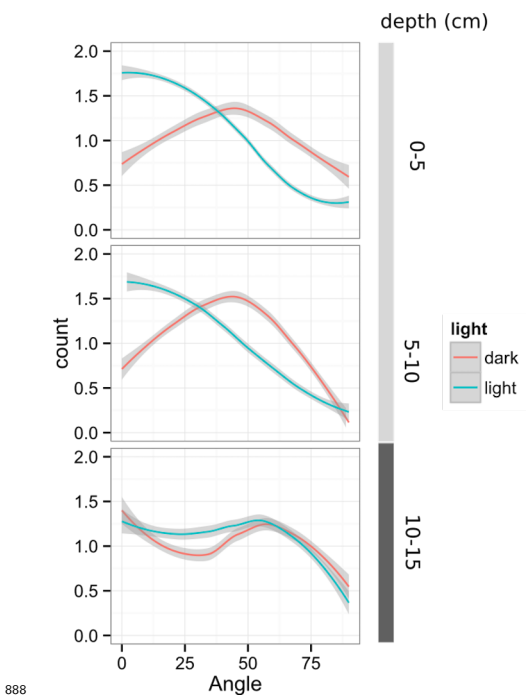
864 **Figure 6-figure supplement 2. Phosphorus deficiency response of root systems**

865 Shoot and root systems of *ProUBQ10:LUC2o* Col-0 plants growing in soil supplemented  
 866 with 1ml of 100 µM P-Alumina (left) and 0-P-Alumina (right) 22 (A) or 27 (B) DAS. C)  
 867 Root depth/width ratio of 22 (top) and 27 (bottom) DAS plants. D) Scatter-plot showing  
 868 relationship between root and shoot system area at 22 (top) and 27 (bottom) DAS. E)  
 869 Root directionality distribution in plants 22 (top) and 27 (bottom) DAS. Anova analysis at  
 870 p < 0.01 was used to compare depth/width ratios in P treatments. Kolmogorov-Smirnov  
 871 test at p < 0.001 was used to compare directionality distributions between the different  
 872 treatments. A Local Polynomial Regression Fitting with 95% confidence interval (grey)  
 873 was used to represent the directionality distribution curve.(0° is the direction of the gravity  
 874 vector).

875

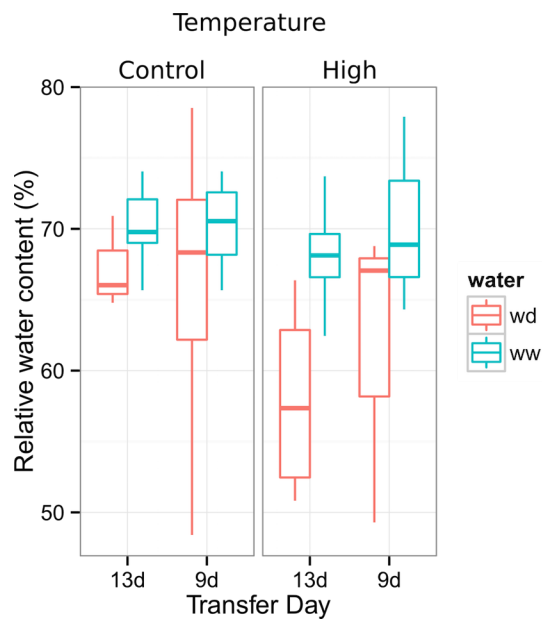


878 **Figure 6-figure supplement 3. Effect of light on root directionality.** A) Col-0  
 879 root systems shielded (top) or light exposed (bottom). After 9 DAS the top third of the  
 880 rhizotron was exposed to light (indicated on the side with a light grey bar) and plants were  
 881 imaged at 20 DAS. B) Directionality analysis of root systems shielded (red) or exposed  
 882 (green) to light for Col-0 (top panel) or *pht1/2* double mutant (bottom panel). Between  
 883 4 and 6 plants were analyzed per treatment. ANOVA analysis at  $p < 0.01$  was used to  
 884 compare depth/width ratios in P treatments. Kolmogorov-Smirnov test at  $p < 0.001$  was  
 885 used to compare directionality distributions between the different treatments. A Local  
 886 Polynomial Regression Fitting with 95% confidence interval (grey) was used to represent  
 887 the directionality distribution curve.(0° is the direction of the gravity vector).



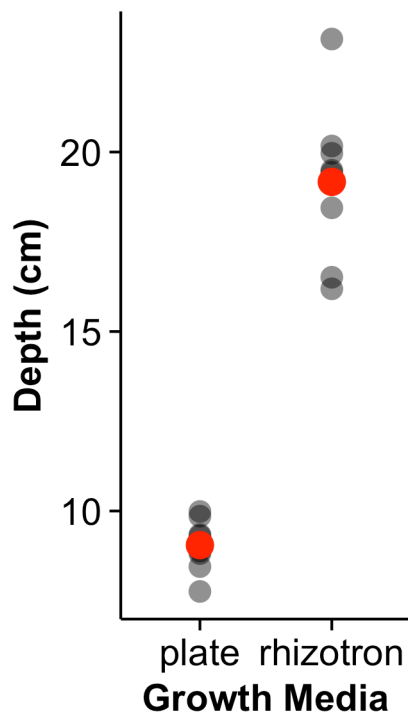
888 **Figure 6-figure supplement 4** Plots showing output of directionality analysis performed  
 889 at different depths (0-5, 5-10, 10-15 cm) in rhizotrons exposed to light or kept in the dark.  
 890 (0° is the direction of the gravity vector).  
 891

892



893     **Figure 6-figure supplement 5.** Leaf relative water content of 23 DAS plants that  
 894     were subjected to water deprivation (WD) after 9 or 13 DAS or kept under  
 895     well watered (WD) conditions. At 9 DAS half of the plants were kept under control  
 896     temperature conditions (22 °C) and the other half transferred to a 29 °C (high) chamber. n  
 897     = 6-8 plants.  
 898

899



901 **Figure 8-figure supplement 1** Depth of the primary root of *Brachypodium* plants grown  
902 in rhizotrons or on gel-based media (n=8-11).

903

904    **Supplementary material**

905    **Supplemental Material 1**

906    Blueprints of the holders, clear sheets and spacers needed to built the rhizotrons. Additional  
907    details are provided in the materials and methods. Files are provided in Adobe Illustrator  
908    .ai and Autocad .dxf formats.

909    **Supplemental Material 2**

910    Primers used in the qPCR experiment.

911    **Supplemental Material 3**

912    Vector maps of all the constructs used in this work.

913    **Source data files**

914    Source data files used for building the following figures are provided: figure\_1D.csv

915    figure\_1\_figure\_supplement\_1A-B.csv

916    figure\_1\_figure\_supplement\_1C\_D.csv

917    figure\_1\_figure\_supplement\_1E-F.csv

918    figure\_1\_figure\_supplement\_2.csv

919    figure\_1\_figure\_supplement\_3.csv

920    figure\_2C.csv

921    figure\_2D.csv

922    figure\_3D.csv

923    figure\_3E.csv

924    figure\_3F-G\_1.csv

925    figure\_3F-G\_2.tps

926    figure\_3\_figure\_supplement\_1A-B.csv

927    figure\_4G\_reporter.csv

928    figure\_4G\_root\_segment.csv

929    figure\_4\_figure\_supplement\_1.csv

930 figure\_4\_figure\_supplement\_2.csv  
931 figure\_5\_figure\_supplement\_1.csv  
932 figure\_6\_A-D.csv  
933 figure\_6\_figure\_supplement\_2-C-D.csv  
934 figure\_6\_figure\_supplement\_2-E.csv  
935 figure\_6\_figure\_supplement\_3.csv  
936 figure\_6\_figure\_supplement\_4.csv  
937 figure\_6\_figure\_supplement\_5.csv  
938 figure\_7.csv  
939 figure\_8\_figure\_supplement\_1.csv